
MULTIPLE INSTANCE VERIFICATION

A PREPRINT

Xin Xu, Eibe Frank, Geoffrey Holmes

Department of Computer Science
University of Waikato
Hamilton, New Zealand

xinxu75@gmail.com, {eibe, geoff}@waikato.ac.nz

November 30, 2023

ABSTRACT

We explore multiple-instance verification, a problem setting where a query instance is verified against a bag of target instances with heterogeneous, unknown relevancy. We show that naive adaptations of attention-based multiple instance learning (MIL) methods and standard verification methods like Siamese neural networks are unsuitable for this setting: directly combining state-of-the-art (SOTA) MIL methods and Siamese networks is shown to be no better, and sometimes significantly worse, than a simple baseline model. Postulating that this may be caused by the failure of the representation of the target bag to incorporate the query instance, we introduce a new pooling approach named “cross-attention pooling” (CAP). Under the CAP framework, we propose two novel attention functions to address the challenge of distinguishing between highly similar instances in a target bag. Through empirical studies on three different verification tasks, we demonstrate that CAP outperforms adaptations of SOTA MIL methods and the baseline by substantial margins, in terms of both classification accuracy and quality of the explanations provided for the classifications. Ablation studies confirm the superior ability of the new attention functions to identify key instances.

Keywords Multiple Instance Learning, Verification, Siamese Neural Networks, Attention, Explainability

1 Introduction

In multiple instance (MI) verification, each exemplar for machine learning consists of a pair of two objects—a query instance and a bag of target instances—and a binary class label that indicates whether or not the bag contains an instance pertaining to the same (unobservable) class as the query instance.¹ Figure 1a shows an example: a synthetic task based on an extended version of the MNIST data consisting of digits and their writers’ ID [38]. In this task, each exemplar contains multiple instances of the same digit written by different writers. The question is whether the target bag contains handwritten digits from the writer who wrote the query—and if there are any, which ones are “key instances”. Other practical applications are illustrated in Figures 1b (signature verification) and 1c (fact verification) respectively. Such tasks are of practical importance because they represent settings that require “verification with noise”. While basic verification tasks involve comparing a query instance to a single target instance, real-world targets available for verification are often “noisy” in the sense that they consist of multiple candidates, some irrelevant, to be compared. Importantly, which individual target instances are relevant is unknown, possibly because obtaining labels of relevancy is too costly. Hence, verification needs to be conducted using the noisy target objects. Note that this generally involves establishing the candidate instances’ relevance to the outcome of the verification process as well—a potentially very useful byproduct.

Conceptually, the MI verification problem may be characterized as a combination of two sub-problems: verification [2] and multiple instance learning (MIL) [10]. Verification is frequently formulated as a binary classification task based on a pair of inputs, predicting whether or not the paired inputs are of the same class. The standard solution is to

¹For brevity, we refer to these components as “query”, “target bag”, “exemplar label”, and “query class”, respectively, in what follows.

²Signatures in Figure 1b are made up and for illustration only, due to data use compliance requirements.

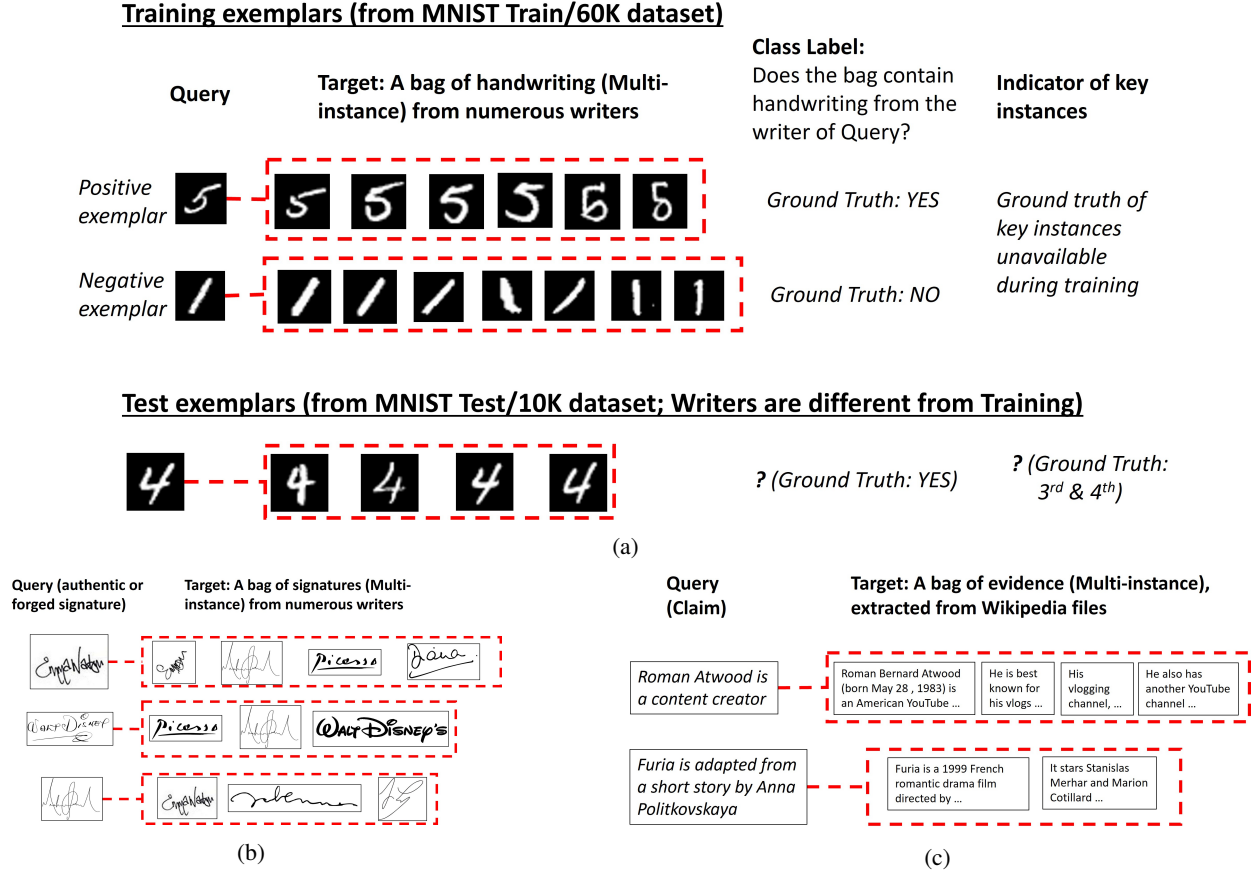


Figure 1: MI verification tasks, with examples from computer vision (CV) and natural language processing (NLP): (1a) verifying handwritten digits (QMNST); (1b) signature verification (displayed signatures are for illustration only, *not* the actual data used in our experiments²); (1c) fact extraction and verification (FEVER).

apply Siamese neural networks [2, 6, 20], but they have no built-in mechanism to aggregate or select from multiple elements within an input, which renders them unsuitable for MI verification. On the other hand, algorithms for MIL, where bags of instances are to be classified, address the ambiguity in how a bag-level class label is related to the unknown labels of the instances in a bag [3, 44]. However, existing MIL methods do not provide a dedicated mechanism to take the information provided by a query instance into account. In this paper, we argue that new algorithms and models are required for this setting and provide theoretical and empirical evidence showing the benefit of explicitly incorporating both components—the target bag and the query instance—and modelling their relationship during learning and inference.

We also stress that “multiple instance verification” and similar terms as used in domains such as biometrics [23, 32] refer to problems that differ from the setting considered in this paper. In those problems, all instances of a bag, by definition, have *homogeneous* unobservable labels, implying no noise or irrelevant elements in the bag for verification. This is in contrast to the verification problem with *heterogeneous* instance labels studied in this paper. Crucially, just as in standard MIL, an exemplar label only provides information about the existence of key instances in a bag but does not identify them. Moreover, as the query instance may belong to a class that has not been observed when the verification model was trained, it enables classification into previously unknown classes. Following the rationale of [20], this is analogous to an MI version of zero-shot classification.

A straightforward approach to MI verification is to combine existing verification and MIL methods as building blocks, e.g., by creating a bag-level representation for the target bag using a state-of-the-art (SOTA) MI pooling method, and then treating this bag-level representation together with the query instance as the two inputs to a Siamese network for verification. Suitable SOTA MI pooling methods include approaches based on gated attention (“gated-attention-based MIL” [17]), the transformer decoder (“Pooling by Multi-head Attention” [21]), and the transformer encoder (e.g., “TransMIL” [30]). Alternatively, one may apply non-attention-based methods such as MI-Net [36] and bi-

direction LSTM (Bi-LSTM) [35]. However, we show that MI verification based on this straightforward approach, regardless of which of the above MIL algorithms is applied, yields unsatisfactory classification performance. More specifically, a simplistic “baseline” model is shown to outperform the resulting instantiations—henceforth referred to as “benchmarks”—of the straightforward approach to MI verification.

We postulate that the benchmarks perform unsatisfactorily because they do not incorporate the query instance into the bag-level representation of the target bag: the “query” concept does not exist in the underlying MIL methods. Indeed, we show theoretically, using a probabilistic interpretation of attention scores, that failure to incorporate the query instance induces less effective attention scores. Hence, inspired by the “query-key-value” attention mechanism of the transformer decoder [34], we propose a new pooling approach called “cross attention pooling” (CAP) that creates the bag-level representation of a target bag through a cross-reference attending to the query. This means the bag’s representation is dynamic because it varies when a different query instance is present, even if the bag itself does not change. In contrast, standard MIL methods create a static bag-level representation. CAP also enables the introduction of two novel attention functions, namely “distance-based attention” and “variance-excited multiplicative attention” respectively, to address the challenge that the instances in a bag may be difficult to distinguish. Both functions accommodate multi-head formulations popular in transformers.

In addition to classification accuracy, the ability to identify the key instances in a target bag is also highly desirable for MI verification. This ability is commonly known as “explainability” or “interpretability” in the literature on MIL [17, 30]. Following recent work on this topic [5, 18], we quantitatively evaluate explanation quality for the methods in our study. This is possible for those datasets where ground-truth instance labels are available.

Our experimental results, obtained from three different tasks and considering both classification and explanation performance, show that CAP is an effective solution to the MI verification problem. In terms of (bag-label) classification performance, it significantly outperforms the benchmarks and the baseline by large margins. Furthermore, using quantitative measures of explanation quality, we show that it identifies key instances far more accurately than both the benchmarks and the baseline. Higher classification accuracy and explanation quality are observed with different numbers of training exemplars and with varying bag sizes in the training data. We also present an ablation study showing that the components of the novel attention mechanisms responsible for delivering superior explanation quality—and thus leading to better bag-level representations—are the source of better classification performance.

Our key contributions are as follows. First, we formally state the MI verification problem, and create a new solution, CAP, that outperforms SOTA MIL methods combined with Siamese networks and a simple baseline method on three tasks from the computer vision (CV) and natural language processing (NLP) domains. Furthermore, we propose two new attention functions for CAP: (a) distance-based attention, which differs from the mainstream functional forms of attention because it is neither additive nor multiplicative, and (b) variance-excited multiplicative attention, which is a new form of multiplicative attention. We show that they are better able to identify key instances in MI verification, resulting in better bag-level representations. While attention-based methods are not uncommon in MIL-related domains, research studying different types of attention mechanism and analyzing their efficacy under specific conditions is rare. Within this context, we provide insights that highlight the importance of quantitative evaluation of the explanation quality to identify spurious model performance. We find that MI models may identify key instances incorrectly but still classify the corresponding bag correctly, and vice versa. The work also contributes to the specific application areas we consider. For example, in the natural language inference (NLI) subtask of “fact extraction and verification”, the existing approach is a two-step pipeline: evidence retrieval and support verification. Our approach combines them into a single step through CAP, and thus enables the end-to-end training of the whole pipeline.

2 Related work

The most closely related existing work is research on verification using Siamese neural networks and the deep MIL literature.

The verification problem, and its solution using Siamese neural networks, was first introduced by the pioneering work of [2]. [6] further explored Siamese networks for similarity metric learning. Since then, the problem settings of verification have been generalized, in both CV (e.g., [41]) and NLP (e.g., [7]) domains where Siamese networks can be applied. There are also several areas in machine learning that apply Siamese networks to solve problems similar to verification, including one-shot learning [15, 20], self-supervised and contrastive learning [4, 42], embedding pre-training [7, 28], to name a few examples.

We note that there exist approaches other than Siamese networks that may also be applicable to MI verification in specific application scenarios, such as using concatenation of the query instance and the target bag in the NLP task considered in [29]. We do not consider this approach here because it needs to be used jointly with other NLP techniques

and cannot be trained end-to-end. Within the scope of this paper, we only consider Siamese networks, which provide a more generic and domain-agnostic approach.

As for MIL, starting from the seminal work of [10], it forms an important area called “weakly supervised learning” (see [44]). Loosely speaking, depending on whether a method (1) explicitly creates a bag-level representation or (2) directly aggregates instance-level scores such as logits, MIL methods may fall into two categories: bag-level and instance-level approaches (see [3]). While many methods from earlier MIL research are instance-level, e.g., [37, 43], later research typically focused on bag-level methods, e.g., [22, 35, 36]. More recently, mainstream deep MIL research has been dominated by attention-based methods [17, 21, 30], which can be viewed as both bag-level and instance-level methods. The attention scores can be viewed as a weighting function that not only aggregates instance-level representations into bag-level ones, but also aggregates instance-level scores. These methods are the focus of our study and are used to derive the benchmark models.

There are also sub-domains of MIL that indirectly relate to our paper. One strand of research considers dynamic representations of bags and models the context of instances [22, 39, 45]. Unlike our study, the focus of this strand is to model the contextual information *within* a bag, rather than information from *outside*. Another strand emerging more recently considers the interpretability of weakly supervised learning, proposing evaluation metrics that do [5, 18] or do not [12] require (unobservable) instance labels. We focus on the former metrics in this paper.

Like recent MIL [21, 30] and other [11, 28] research, our methods are also strongly inspired by the transformer architecture [34] and can be grouped with the wider range of research that is based on this seminal model. Indeed, many CV or NLP problems solved by transformers can be represented as MIL problems with sequentially ordered instances, in which the sequence order can be addressed by the addition of positional embedding (see, e.g., [30]).

Finally, there are specific areas of CV and NLP that are related to our work. Examples in CV include weakly-supervised object detection/localization [5, 18] and one-shot object detection [15]. In NLP, one area is “fact extraction and verification” (“FEVER”, see [33]). It is well-suited to the MI verification framework because of the framework’s ability to deal with ambiguity. Indeed, we evaluate our approach on one of the FEVER datasets.

3 MI verification: problem definition and an interpretation of attention scores

The scenario of “verification with noise” is applicable to many tasks in the areas of CV and NLP. To give a few examples, practical use cases of MI verification include:

- verification of whether a document (bag of paragraphs) has content generated by a particular writer based on a writing sample (paragraph) of this writer;
- verification of whether a video clip (bag of images) contains targets such as people, endangered species, plants, etc., specified by a reference image;
- verification of whether a medical image (bag of patches) indicates certain diseases like Covid-19, cancer, etc., based on a known disease image patch. A generalization of this use case relates to the broader subject of “weakly-supervised one-shot object detection” in the CV domain;
- verification of whether a network log (bag of scripts or time series) records traces of cyber-attacks based on the footprint of a past attack, and so on and so forth.

It is also worth noting that, while standard information retrieval tasks, i.e., searching for content relating to a query, can usually be addressed by classic verification methods, MI verification relates to *non-standard*, weakly-supervised “cross-domain” retrieval tasks where content is suitably represented as a bag of multiple and ambiguous instances. For example, the first two examples above—retrieving a document based on a paragraph, or retrieving a video based on an image—are relevant use cases.

3.1 Three example MI verification tasks

To enable a better understanding of MI verification and its usefulness, we first present detailed information on the three MI verification tasks illustrated in Figure 1. These are tasks for which we were able to obtain publicly available data for our experiments.

To generate the exemplar labels for handwriting verification (Figure 1a), we used an extended version of MNIST, the QMNIST dataset [38], which includes the writer IDs of all the handwritten digits in the MNIST dataset. To differentiate our task from the standard MNIST classification task of digit recognition, and to focus on the query class (i.e., the writer ID), we constructed each exemplar using the same digit across the entire exemplar comprising the query and the target bag. To avoid trivial cases that the query is also in the bag, we ensured that all images in the bag are different

from the query even if they may be written by the same writer. Note that the “inference” stage in Figure 1a depicts the two goals of our study: verification and explanation.

In the signature verification task (Figure 1b), a target bag is composed of multiple authentic signatures, usually called “anchor” images. There are three types of query signature:

1. an authentic signature that can be verified by some anchors in the target bag (i.e., the query and anchors are written by the same writer),
2. a professionally forged signature that looks similar to some anchors, and
3. an unmatched signature that does not look close to any anchor.

The (unobservable) query class is the writer ID. The exemplar’s label signals whether or not the query can be verified as authentic by any anchor in the target bag. Thus, it is “1” for the first case and “0” for the second and third cases considered in the above list.

In the FEVER task (Figure 1c), the target bag consists of multiple pieces of evidence, each represented by paragraphs extracted from various Wikipedia pages, and the query is a claim about a fact. The (unobservable) query class is the semantic category of the query paragraph (determined by human experts): supportive of the claim or unsupportive. By construction, any query is “supportive” of itself. If a piece of evidence in the target bag is supportive, the query is said to be supported by the evidence, i.e., they are of the same query class. Thus, the exemplar’s label is whether or not the query is supported by any evidence in the target bag.

For all three tasks described above, we were able to collect identifiers of the key instances, either by construction or from raw data. This information is used during testing, to evaluate the explanation quality of the models, but not during training.

3.2 Formal definition of MI verification

To formally state the task of MI verification, we use the following notation. The (unobservable) class label of an instance x is denoted by $y \in c$ where $c = \{1, 2, \dots, L\}$ and L is the number of unobservable classes. Note that L can be ∞ . The query instance and its unobservable class label are denoted by x_Q, y_Q , and the bag of target instances and their unobservable class labels by $\{x_1, x_2, \dots, x_N\}$ and $\{y_1, y_2, \dots, y_N\}$ respectively. Unless stated otherwise, in this section, we assume the instances, $x_Q, x_n (n = 1, \dots, N)$, have all been embedded in an F -dimensional feature space, that is, $\in \mathbb{R}^F$.

Definition 1 (MI verification exemplar). *An MI verification exemplar is a tuple, $(x_Q, \{x_1, x_2, \dots, x_N\})$, with a label Y given by*

$$Y = \begin{cases} 0, & \text{iff } y \neq y_Q \quad \forall y \in \{y_1, y_2, \dots, y_N\} \\ 1, & \text{otherwise.} \end{cases}$$

It is worth noting that an MI verification task can be converted into a “multiple pairs-of-instances” learning problem, analogous to MIL, by pairing the query instance with each instance in the target bag. We state this formally as a lemma below.

Lemma 1 (Conversion of MI verification exemplars). *An MI verification exemplar in Definition 1 can be represented as a bag of paired instances $\{(x_Q, x_1), (x_Q, x_2), \dots, (x_Q, x_N)\}$, each with an unobservable binary class label $\hat{y}_n \in \{0, 1\}, n = 1, 2, \dots, N$ defined as*

$$\hat{y}_n = \begin{cases} 0, & \text{iff } y_n \neq y_Q, \quad n = 1, 2, \dots, N \\ 1, & \text{otherwise.} \end{cases}$$

The bag label is given by

$$Y = \begin{cases} 0, & \text{iff } \sum_n \hat{y}_n = 0 \\ 1, & \text{otherwise.} \end{cases}$$

The proof is trivially obtained by construction.

3.3 Permutation invariance in MI verification

In MI verification problems, like classic MIL, the order of the instances in a bag should not matter—the function used to score bags of data should be permutation-invariant. Lemma 1 allows us to borrow theory from existing MIL literature, e.g. [17, Theorem 1], to provide a sufficient and necessary condition for the scoring function, $S(X)$, of a bag of instance-pairs to be permutation invariant. We state this formally in Lemma 2, simply replacing an instance x_n with a pair of instances (x_Q, x_n) in [17, Theorem 1].

Lemma 2 (Condition for permutation invariance). *A scoring function, $S(X) \in \mathbb{R}$, for a set of pairs $X = \{(x_Q, x_1), (x_Q, x_2), \dots, (x_Q, x_N)\}$, is permutation invariant to the elements in X , if and only if it can be decomposed in the following form*

$$S(X) = g\left(\sum_{(x_Q, x_n) \in X} f(x_Q, x_n)\right), \quad n = 1, 2, \dots, N \quad (1)$$

where f and g are suitable transformations.

Lemma 2 allows us to demonstrate that the models under the CAP framework, introduced in Section 4.1, are permutation invariant. As we will see, the models in Section 4.1 use a scoring function that can be written as

$$S(X) = H(x_Q) \text{diag}(\alpha) \text{concat}_{j=1, \dots, h} \left(\sum_n^N (A_j(x_Q, x_n) G_j(x_n)) \right)^T,$$

where $\text{concat}_{j=1, \dots, h}$ concatenates h vectors (one from each attention head), $A_j(x_Q, x_n) \in \mathbb{R}$ is a scalar attention score for the n^{th} instance in the target bag at the j^{th} head, $H(x_Q) \in \mathbb{R}^{1 \times F}$, $G_j(x_n) \in \mathbb{R}^{1 \times \frac{F}{h}}$ are transformations of x_Q and x_n (at the j^{th} head) respectively, and $\text{diag}(\alpha) \in \mathbb{R}^{F \times F}$ is a diagonal matrix of learnable parameters.

We can split the vectors $H(x_Q)$ and α into h equal-length segments, and rewrite this scoring function by moving $H(x_Q)$ and $\text{diag}(\alpha)$ inside the summation,

$$\begin{aligned} S(X) &= \sum_j^h \left[\sum_n^N A_j(x_Q, x_n) \left(G_j(x_n) \text{diag}(\alpha_j) H_j(x_Q)^T \right) \right] \\ &= g\left(\sum_n^N f(x_Q, x_n)\right), \end{aligned} \quad (2)$$

where $H_j(x_Q) \in \mathbb{R}^{1 \times \frac{F}{h}}$, $\alpha_j \in \mathbb{R}^{\frac{F}{h}}$ denote the j^{th} segment of the corresponding vectors.

The first line of Equation (2) states that the logit of our models is the sum of “sub-logits” from multiple heads. The sub-logit from each head is the attention-score weighted sum of N Siamese-twin similarities computed from N pairs, where each pair is formed by the query (transformed by H) and the corresponding instance in the target bag (transformed by G)—conforming to the conversion process in Lemma 1. The last line is obtained by simply treating \sum_j^h as $g(\cdot)$, and everything inside the summation \sum_n^N as $f(\cdot, \cdot)$.

Although with theoretical merits, the results in this section are not particularly helpful in guiding us to find specific functional forms of $S(X)$. Indeed, even naive employment of existing SOTA MIL attention mechanisms may fit with Lemma 1 and 2. Intuitively, this naive approach may be problematic because these mechanisms do not account for the special role of the query instance. To substantiate this intuition, we need a new framework for interpreting attention scores.

3.4 A probabilistic interpretation of attention scores

We present a probabilistic interpretation of attention scores based on the observation that they are non-negative and sum to 1. Therefore, they form a probability distribution $Pr(U)$ of a discrete random variable $U \in \{n \mid n = 1, 2, \dots, N\}$ that encodes the relevance to the exemplar label of the N instances it contains. This enables the use of two concepts from probability theory. First, the attention-weighted sum of the instances’ feature vectors can now be seen as an expectation, where this expected vector represents the entire bag. Second, the entropy $H(U)$ of $Pr(U)$ can be used to measure the informativeness of a set of attention scores—large entropy corresponds to an even distribution of attention scores, which provides little information about the relevance of individual instances to the bag’s label—and well-known properties from information theory [8] can be applied.

The probability distribution for a particular MI verification exemplar clearly depends on the information in the query instance and the target bag. We assume that the query instance and the instances in the target bag have all been embedded in an F -dimensional feature space, yielding $V^{Query} \in \mathbb{R}^F$ and $V^{Target} \in \mathbb{R}^{N \times F}$. It can be shown that, under mild conditions, we can *strictly* reduce uncertainty, and thus *strictly* increase informativeness regarding the key instances in a target bag, by considering information from both sources, V^{Target} and V^{Query} , rather than just one. We state this as Proposition 1, together with Assumption 1, as follows.

Assumption 1 (Uncertainty of conditioning variables’ informativeness).

$$Pr\left(H(U | V^{Query}) > H(U | V^{Target})\right) > 0, \quad (3)$$

$$Pr\left(H(U | V^{Query}) < H(U | V^{Target})\right) > 0.$$

Assumption 1 states that informativeness of attention scores brought by V^{Query} and V^{Target} should be uncertain, that is, there should be no guarantee that one variable is more informative than another, and vice versa—any scenario is possible with nonzero probability.³ This rules out any special condition or constraint on the marginal informativeness of any conditioning variable. In practice, it is a reasonable assumption because it is generally impossible to say with certainty that any given information source is more or less informative than any other.

Proposition 1 (Variables incorporated in the attention scores). *Assuming that all random variables are valued in standard Borel spaces and Assumption 1 holds,*

$$H(U | V^{Target}) > H(U | V^{Query}, V^{Target}) \quad (4)$$

$$H(U | V^{Query}) > H(U | V^{Query}, V^{Target}) \quad (5)$$

See Appendix A for the proof.

In particular, conditioning on V^{Target} alone can only reduce the ability to identify key instances correctly. This is important because tackling MI verification using naive combinations of Siamese networks and SOTA attention-based MIL models does not incorporate the information from the query into attention. In contrast, our approach uses both the query instance and the target bag to model the attention scores, and Proposition 1 provides a theoretical foundation for it.

4 Model architectures

We now describe the different modelling approaches to MI verification that we compare in our study, including the two attention functions used in the new approach based on cross-attention pooling (CAP).

The baseline, benchmark, and CAP-based models compared in our study share the same architecture for the first two layers and the final two layers of the neural networks. In the first two layers, we obtain fixed-length feature vectors by embedding the query instance and all instances in the target bag using appropriate feature extractors from the CV or NLP domains, as required by the application at hand, followed by a layer normalization (LayerNorm) [1]. We denote the feature vectors *after* LayerNorm as $v^{query} \in \mathbb{R}^{1 \times C}$ and $v^{target} \in \mathbb{R}^{N \times C}$ respectively, where N is the number of instances in a bag (“bag size”), and C is the number of channels. Note that bag size N varies across exemplars. For the final layer, regardless of architecture, we adopt a binary cross-entropy loss, in which each exemplar’s prediction is $p = \text{sigmoid}(\text{sim})$, where sim is a Siamese-twin similarity score:

$$\text{sim} = \sum_{i=1}^C \alpha_i f(v_i^P, v_i^Q), \quad (6)$$

where $\alpha \in \mathbb{R}^{1 \times C}$ is a vector of learnable parameters, and $v^Q, v^P \in \mathbb{R}^{1 \times C}$ are the two outputs of the Siamese twins, corresponding to (a) the encoded query instance and (b) the bag-level representation, which is the attention-weighted sum of the encoded target bag instances, respectively (*cf.* Figure 2). The function $f(v_i^P, v_i^Q)$ measures the similarity between v^P and v^Q . Equation (6) is the same as that used by [20], except that we use the product function, $f(v_i^P, v_i^Q) = v_i^P v_i^Q$ instead of L_1 distance, which yields

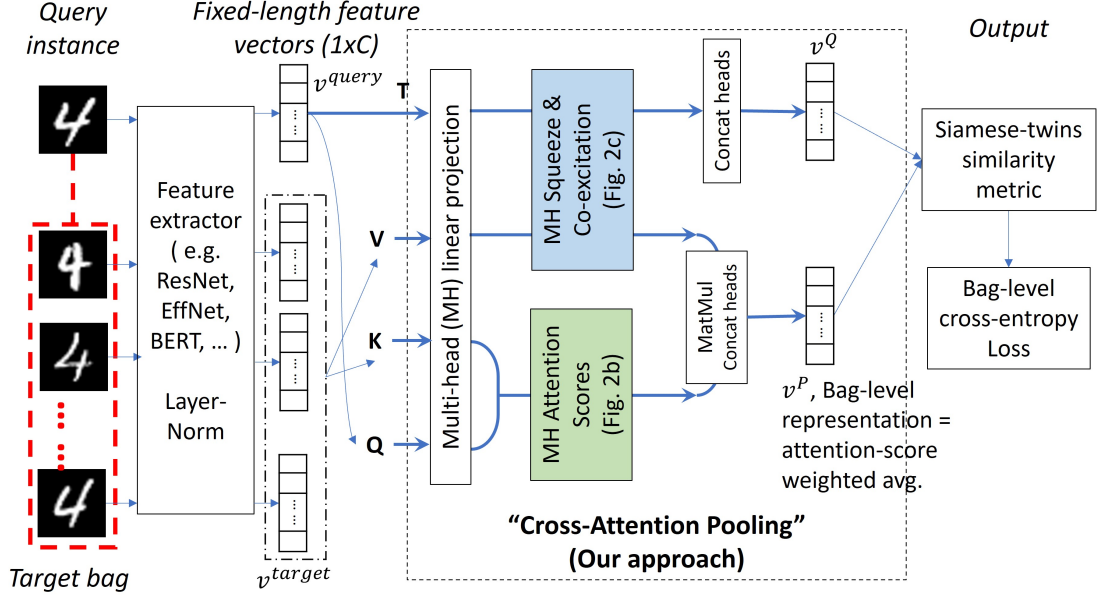
$$\text{sim} = v^Q \text{diag}(\alpha) (v^P)^T, \quad (7)$$

where $\text{diag}(\alpha)$ denotes a $(C \times C)$ diagonal-matrix based on α .

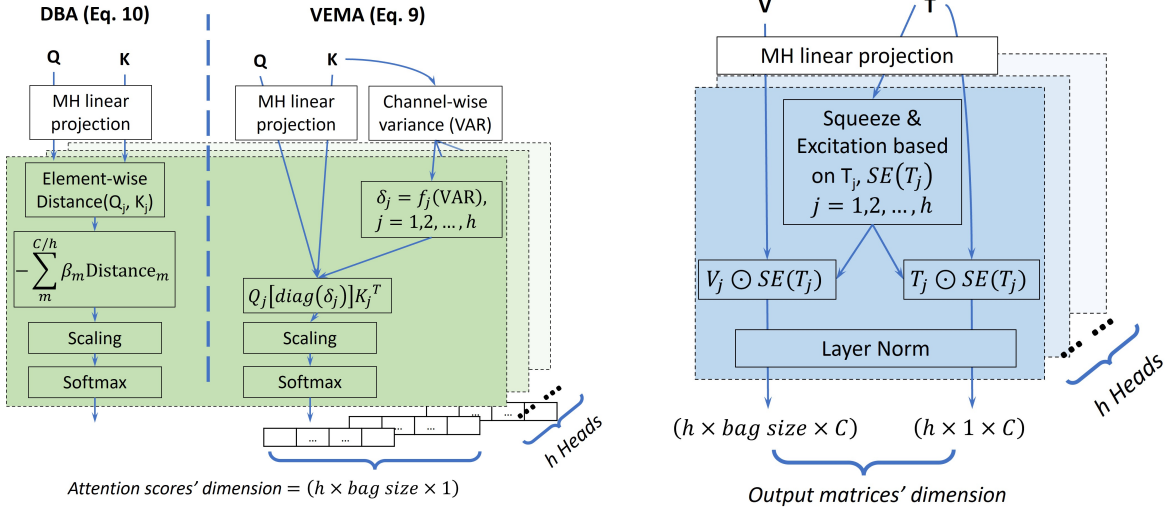
4.1 Our approach: Cross Attention Pooling

The main difference between the Siamese networks investigated in this study is how they perform MI pooling of v^{target} to get v^P . Our new pooling method CAP is motivated by two considerations. First, as implied by Proposition 1, it is

³Note this probability is well-defined because a conditional entropy is a random variable.



(a) CAP architecture



(b) Multi-head attention scores

(c) Multi-head squeeze and co-excitation

Figure 2: Model architecture for ‘‘Cross Attention Pooling’’, shown in (2a), and its key components: (2b) multi-head attention scores and (2c) squeeze & co-excitation, best viewed in colour.

strictly better to incorporate v^{query} to model attention scores for the pooling of v^{target} . To operationalize this idea, we construct the attention score for each instance in the target bag (v^{target}) by attending it to v^{query} as a cross-reference, inspired by the “query-key-value” framework in the transformer decoder [34].

The second consideration comes from the challenge of handling tasks in which all instances in a bag look alike, exemplified by the QMNIST problem in this study. The challenge is how to make key instance(s) stand out among similar-looking instances, through an uneven distribution of their attention scores. We tackle this using two strategies. One is to create new functions that provide unevenly distributed attention scores. Another is to adjust channels of the “value”-vector. The former gives rise to our novel attention functions, namely variance-excited multiplicative attention (VEMA) and distance-based attention (DBA). The latter leads to our multi-head adaptation of “squeeze and co-excitation” [15], a variation of the “squeeze and excitation” network [16].

Figure 2 depicts the entire Siamese network architecture, including our CAP approach highlighted by the dotted rectangle (Figure 2a), together with its key components for computing attention scores (Figure 2b) and “squeeze and co-excitation” (Figure 2c) highlighted by green and blue colours respectively—those components are explained more formally in Section 4.1.2 below. As shown in the figure, there are two outputs of CAP: one is the bag-level representation v^P , another is the transformed query instance v^Q . v^P is a function of the triad of “query, key, value” denoted by “ $\mathbf{Q}, \mathbf{K}, \mathbf{V}$ ”, whereas v^Q is a function of v^{query} denoted by “ \mathbf{T} ”, in the figure. The functions producing v^P and v^Q are formally specified by Equation (8) as follows.

4.1.1 Multi-head Cross Attention Pooling

Letting $\mathbf{Q} = v^{query}$, $\mathbf{K} = \mathbf{V} = v^{target}$, $as(\cdot, \cdot)$ be the attention-score function, $LN(\cdot)$ be layer normalization, $MHSCE(\cdot)$ be “multi-head squeeze and co-excitation”, we model the outputs of the Siamese twins as

$$v^P = \text{concat}(O_1^P, O_2^P, \dots, O_h^P), \quad v^Q = \text{concat}(O_1^Q, O_2^Q, \dots, O_h^Q),$$

$$O_j^P = \text{MatMul} \left[\underbrace{as_j(v^{query} W_j, v^{target} W_j)}_{1 \times N}, \underbrace{LN_j(v^{target} W_j \odot MHSCE_j(v^{query}))}_{N \times D} \right], \quad (8a)$$

$$O_j^Q = \underbrace{LN_j(v^{query} W_j \odot MHSCE_j(v^{query}))}_{1 \times D}, \quad j = 1, 2, \dots, h \quad (8b)$$

where h is the number of heads, $D = \frac{C}{h}$, $W_j \in \mathbb{R}^{C \times D}$ are learnable weights of the multi-head linear projections shared by $\mathbf{Q}, \mathbf{K}, \mathbf{V}$, and the subscript j of $as_j(\cdot, \cdot)$, $MHSCE_j(\cdot)$, $LN_j(\cdot)$ indicates the j^{th} head. MatMul and \odot denote matrix and element-wise multiplication respectively.

Next, we provide details of the functions $as(\cdot, \cdot)$ and $MHSCE(\cdot)$ for an individual head within the multi-head setting, omitting the subscript j for brevity.

4.1.2 Components of Cross Attention Pooling

VEMA is one of the two attention functions we propose. The rationale is to construct an adaptation of the existing multiplicative attention popularized by the transformer [34]. Additionally, VEMA creates an adjustment using channel-wise variance (across instances within a bag). Intuitively, when all instances in a bag look similar to each other, channels that make them *more different*, i.e., channels with *higher variance*, may make it easier to identify key instances. Accordingly, we design the “excitation by variance” of channels, which can be viewed as an additional feature selection (or channel selection) mechanism in attention. We expect it to produce more unevenly-distributed attention scores, and hence more accurate predictions of the key instances, a hypothesis to be tested by the experiments in Section 6. Formally, we have

$$as(Y, Z) = \text{softmax} \left(\frac{Y \text{diag}(\delta) Z^T}{\sqrt{D}} \right), \quad (9)$$

where Y and Z have shape $(1 \times D)$ and $(N \times D)$ respectively, and $\delta \in \mathbb{R}^{1 \times D}$. δ is modelled as a gating mechanism, $\delta = \text{sigmoid} \left[\text{relu} \left((\text{variance}(v^{target}) - 1) R \right) S \right]$, where $\text{variance}(v^{target}) \in \mathbb{R}^{1 \times C}$ denotes the channel-wise variance of v^{target} , $R \in \mathbb{R}^{C \times C}$, $S \in \mathbb{R}^{C \times D}$ are learnable parameters (with S projecting channels to a single head), and sigmoid , relu are element-wise activation functions.

Our motivation for the second attention function DBA is to establish an equally effective but simpler alternative to VEMA. Considering multiplicative attention as a generalized “cosine similarity”, we surveyed alternative similarity measures, which led to DBA as a new attention function. More precisely, the attention scores of DBA are driven by

the negative sum of weighted distances between corresponding channels of vectors in \mathbf{K} and \mathbf{Q} . In this paper, we use L_1 -distance, noting that other distance metrics are also possible. The DBA attention-score function is

$$as(Y, Z) = \underset{n \in \{1, \dots, N\}}{\operatorname{softmax}} \left(\frac{c - \sum_m^D \beta_m |Y_{0,n,m} - Z_{0,n,m}|}{s} \right), \quad (10)$$

where Y and Z are broadcast to the same shape ($1 \times N \times D$), $|\cdot|$ yields element-wise absolute value, $\beta \in \mathbb{R}^{1 \times D}$ is a vector of learnable parameters for a single head (with different β for different heads), and $c = \sqrt{\frac{4}{\pi}}D$ and $s = \sqrt{(2 - \frac{4}{\pi})D}$ are two constant scalars, broadcast as ($1 \times N$) to be compatible with Equation (10). Like the scaling factor in the transformer [34], c and s are normalizing factors to maintain numerical stability.⁴ Comparing Equation (10) and (9), we can see that DBA is simpler than VEMA, with fewer learnable parameters (C vs. $2C^2$),⁵ and without additional components other than the L_1 -distance. The effectiveness of this simplification is examined in Section 6.

Finally, to adopt SCE, the same “squeeze” and “excitation” functions are shared in both Equations (8a) and (8b), prior to element-wise multiplications with $(v^{target}W_j)$ and $(v^{query}W_j)$ respectively. We apply SCE in a multi-head context, thus naming it “MHSCE”. More precisely, MHSCE’s “excitation” function is the following gating mechanism, in which $\operatorname{mean}(x) \in \mathbb{R}^{1 \times C}$, denoting the channel-wise mean of x , is the “squeeze” function: $MHSCE(x) = \operatorname{sigmoid} \left[\operatorname{relu} \left(\operatorname{mean}(x)J \right) M \right]$, where $J \in \mathbb{R}^{C \times C}$, $M \in \mathbb{R}^{C \times D}$ are learnable parameters, and $\operatorname{sigmoid}$, relu are element-wise activation functions. We emphasize that the same $x = v^{query}$, as well as the same learnable parameters, in $MHSCE(x)$ are shared between Equations (8a) and (8b), that is, in both Siamese twins. Also note that $MHSCE(\cdot)$ is multi-headed, because M projects all the channels to a head.

4.2 Baseline and benchmark models

To provide a baseline for all models, we create a simple model for MI verification. We also adapt SOTA methods from the MIL literature to develop three benchmark models that enable model comparison. The three SOTA methods are: “gated-attention based MIL” (GABMIL) from [17], “pooling by multi-head attention” (PMA) from [21], and “multi-head self attention” (MSA) used in [11, 30]. While the benchmark models are all attention-based, we also experiment with some non-attention-based MI-pooling methods in Section 6, namely MI-Net [36] and bi-direction LSTM [35]. The architectures of the benchmark and attention-based baseline models are depicted in Figure 3 and explained as follows. The architectures of non-attention-based models are similar to that of the benchmark using GABMIL (Figure 3b)—that is, v^P , the non-attention-based bag-level representation of v^{target} , and $v^Q = v^{query}$ are the two outputs of the Siamese twins—and are omitted here for brevity.

4.2.1 The baseline

The baseline model simply pairs v^{query} with each of the N vectors comprising v^{target} and computes the Siamese-twin similarity metric, in Equation (7), for each pair. It then takes the maximum of the N similarity scores as the logit of this exemplar, to be fed into the activation and loss function, see Figure 3a.

Because the baseline model aggregates a bag based on its elements’ scores without an explicit bag-level representation, it is analogous to an extension of instance-level MIL methods, e.g., mi-Net of [36]. Implicitly, it nevertheless still has a bag-level representation for the target bag, which is the feature vector of the instance whose corresponding pair attains the maximum score. More precisely, the baseline can be viewed as a very simple attention model since taking the maximum implements an attention mechanism using the $\mathbb{1}_{argmax}$ function instead of the $\operatorname{softmax}$ function used by other models, where $\mathbb{1}_{argmax}$ denotes an indicator function providing a vector based on the set of indices returned from the $argmax$ function.⁶ Like in other attention-based methods, the (implicit) bag-level representation in the baseline model is also the attention-score weighted sum of the instances’ representations:

$$v^P = \mathbb{1}_{argmax} \left(v^{query} \operatorname{diag}(\alpha) (v^{target})^T \right) \cdot v^{target},$$

where α is the learnable parameter vector in Equation (7).

This baseline is limited, due to (1) its simplified architecture with very few learnable parameters, (2) the $argmax$ attention function that allows only those instances that yield maxima to represent the entire bag, and (3) parameters α that are shared by both the Siamese-twin metric and the attention mechanism. Nonetheless, this simple model captures the essence of what we call “cross-attention” because it directly includes the query instance v^{query} as part of attention. Hence, this model is a useful baseline for model comparisons.

⁴ c, s are the mean and standard deviation of $\sum_j^D |a_j - b_j|$ assuming all a_j, b_j are i.i.d. $\sim \mathcal{N}(0, 1)$.

⁵The actual implementation of VEMA also includes a bias term, resulting in $2(C^2 + C)$ parameters.

⁶In case there is more than one maximum, the output of $\mathbb{1}_{argmax}$ is normalized by L_1 -normalization to sum to 1, i.e., $\frac{|x_n|}{\sum_n |x_n|}$.

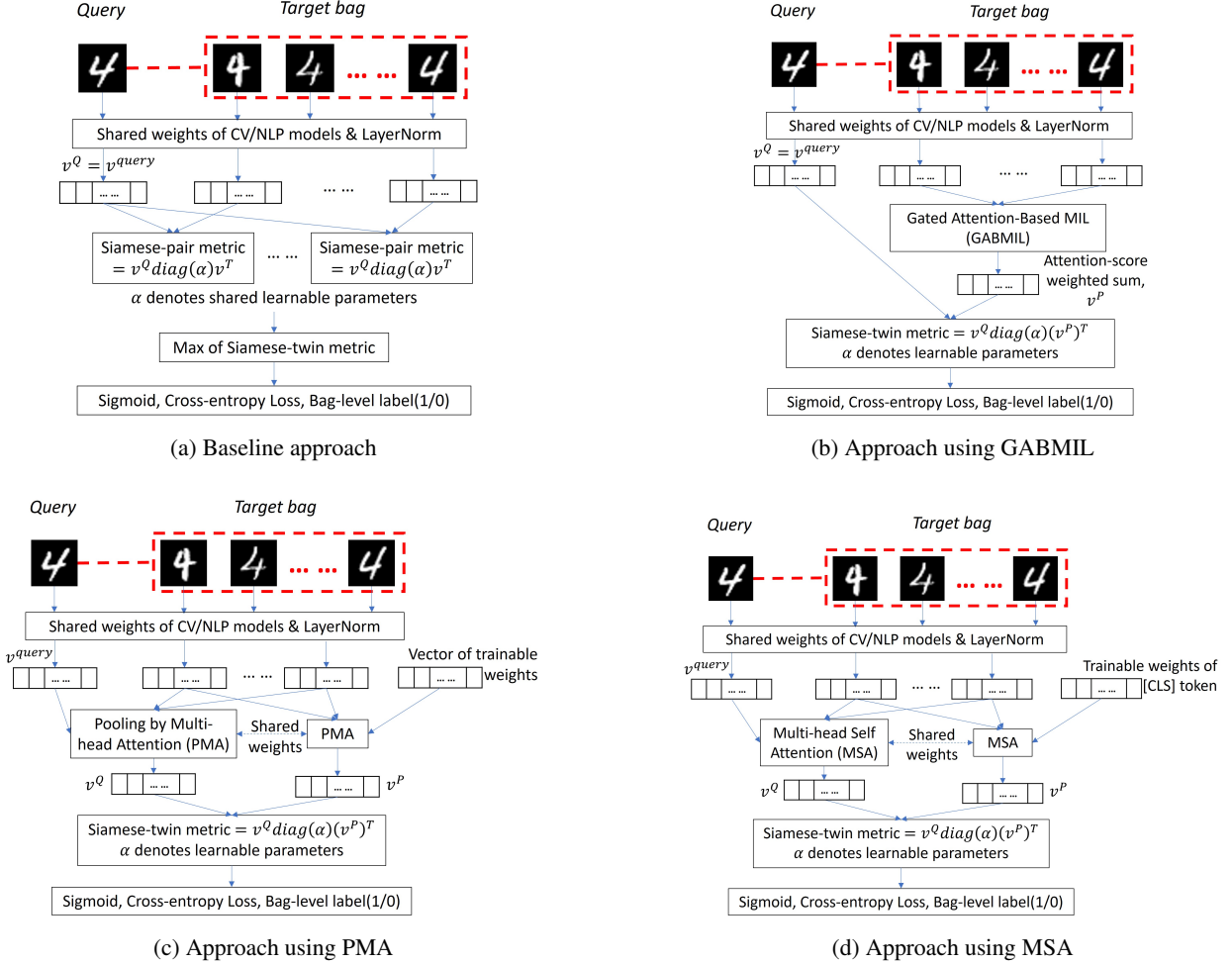


Figure 3: Model architectures of the baseline and the benchmarks

4.2.2 Benchmark using GABMIL

As the first benchmark, we adopt the MI pooling method of Gated-Attention-based MIL (GABMIL) from [17] to aggregate v^{target} , which computes one branch of the Siamese twins v^P as the attention-weighted sum of v^{target} , and another as $v^Q = v^{query}$ (cf. Figure 3b).

4.2.3 Benchmark using PMA

The second benchmark applies an MI pooling method based on the transformer decoder, called “Pooling by Multi-head Attention” (PMA) by [21]. PMA has the same architecture as the transformer decoder (without positional encoding and dropout), used to aggregate v^{target} .

[21] defines PMA_k by applying multi-head attention on a learnable set of k seed vectors $\in \mathbb{R}^{k \times C}$. We initially used PMA_1 to aggregate v^{target} : $v^P = PMA_1(v^{target}; P)$, $v^Q = v^{query}$, where $P \in \mathbb{R}^{1 \times C}$ is a learnable seed vector. However, exploiting the Siamese-twin structure, we found it useful to treat the query’s feature vector v^{query} as another seed vector when computing v^Q . More precisely, we stack v^{query} on P , and compute the outputs of the Siamese twins as follows (see also Figure 3c),

$$(v^P, v^Q) = PMA_2(v^{target}; (P, v^{query})).$$

We found that PMA_2 yields slightly better classification performance than PMA_1 . Therefore, we adopt PMA_2 as the method for the experiments presented in this paper.

Query Target: A bag of handwriting (Multi-instance) from numerous writers

Ground Truth	0	0	1	1	0	} i-AUROC i-AP
Attention Scores						
Baseline	0	0	0	1	0	0.75 0.7
GABMIL	0.209	0.223	0.2	0.29	0.078	0.667 0.75
PMA	0.491	0.014	0.442	0.034	0.019	0.667 0.583
CAP-VEMA (ours)	0.008	0.031	0.232	0.723	0.006	1 1
CAP-DBA (ours)	0.035	0.005	0.12	0.839	0.001	1 1

Figure 4: An illustration of the quantitative evaluation of explanations. Ground-truth key instances, highlighted by red rectangles, are unavailable during training.

4.2.4 Benchmark using MSA

Finally, there is an extensive range of applications and variations of transformer encoders in the literature, e.g., [11, 30]. The key component of these is multi-head self-attention (MSA), characterized by the full self-attention of all the instances within a bag to themselves.

MSA per se cannot aggregate multiple instances, because it retains the same positions in the output sequence as in the input sequence. To use MSA as an MI pooling method, the common practice is to include an additional, special token “[CLS]” in the input sequence, whose embedding vector, $v^{[CLS]}$, is learnable. One can treat the vector at the position of “[CLS]” in the output sequence as the aggregation of the rest of the inputs.

Analogous to PMA_2 , we may treat v^{query} as a feature vector of another special token. We then apply the same MSA (without positional encoding and dropout) twice, on both $v^{[CLS]}$ and v^{query} . This gives rise to the Siamese twins (in Figure 3d) as

$$(v^P, v^Q) = MSA\left(v^{target}; (v^{[CLS]}, v^{query})\right).$$

Following common practice to stack multiple MSA layers when aggregating v^{target} , see, e.g., [30], we stacked two layers of MSA—adding more layers did not appear to add value in our experiments.

We note that none of the three benchmark methods has a natural mechanism to incorporate v^{query} as part of attention when producing the bag-level representation v^P . Even though the Siamese-twin similarity metric may induce a reference to v^{query} in attention-weighted aggregation of v^{target} , this relationship is not modeled explicitly, which may make it less effective for the identification of key instances and for classification. Section 6 provides empirical evidence that supports this hypothesis: the benchmarks are not better, and sometimes significantly worse, than the simple baseline.

5 Evaluating the quality of the explanations

Attention-based MIL models, e.g., [17, 30], reflect the importance of the ability to identify “key instances” using attention scores extracted from models. Following the literature, we also pay attention to the evaluation of explanation quality in the context of MI verification. This is possible when the ground truth of key instances is available in the datasets, as is the case in our study.

Unlike previous literature that considers qualitative demonstrations of explanation quality, this paper focuses on quantitative evaluation. More precisely, for each positive exemplar in the test dataset, we match the ground truth of its key instances’ identifiers to a model’s attention scores. When there are multiple heads, we follow standard practice by averaging the attention scores across all heads to identify the key instances. Figure 4 provides an illustration of such matching for a test QMNIST exemplar. This process is related to evaluation for “weakly-supervised object localization” in CV domains [5, 18], from which we employ two *threshold-independent* ranking metrics, namely pixel “area under ROC curve” (AUROC), and pixel “average precision” (AP).

The threshold independence comes from the definitions of AUROC and AP—they are summary statistics of ROC and PR curves (see e.g., [9]), on which each point evaluates the classification performance based on a single decision threshold. Consequently, by summarizing the entire curves, both metrics measure the performance across all possible classification thresholds and thus are *threshold-independent*. The reasons to require threshold independence in our case are twofold: one, avoid controversies regarding how thresholds are determined to predict key instances (see, for example, [5]); two, for attention models, selecting thresholds may be less straightforward because attention scores must sum to 1, and the bag size N varies across exemplars. Therefore, sensible thresholds may need to be dynamic for exemplars with different sizes, a subject that is beyond the scope of this paper.

We adopt the same computation as pixel AUROC and pixel AP, except that we replace “pixel” with “instance”. Accordingly, we call them instance AUROC (i-AUROC) and instance AP (i-AP), both of which assess explanations for a single exemplar. To summarize the two metrics for the entire test dataset, we take the average of i-AUROC (average i-AUROC) and i-AP (average i-AP), respectively, across all exemplars in the data.

The example in Figure 4 shows that i-AUROC and i-AP accurately reflect quality of the explanations for an individual exemplar—their values are consistent with the rankings of the attention scores with respect to the ground truth of two key instances. More importantly, in this example, all models correctly predict the exemplar label (=1), but the explanation quality differs. Together with more results in Section 6.2, this demonstrates that even if a model misidentifies key instances, it will quite possibly make a correct classification, and vice versa. Therefore, classification performance alone is insufficient to fully evaluate MI models: it should be complemented by quantitative assessment of explanations, whenever possible.

Note that we omit the models adapted from non-attention-based MIL methods when assessing explanations because they are either unable to identify the key instances [36], or require complicated post-processing to do so [35]. We additionally omit the MSA benchmark when evaluating quality of the explanations, for two reasons. One, there is inconsistency regarding how to properly extract attention scores in the literature relating to the transformer encoder. For instance, [11] used “attention rollout” whereas [30] used the final MSA-layer to obtain attention scores. It is not yet clear which way should be adopted. Two, as MSA is not a natural pooling method, its extracted attention scores include components that are irrelevant for MI pooling due to the self-attention mechanism. It is also unclear how to better post-process (e.g., re-normalize) the extracted attention scores to obtain meaningful explanations.

6 Experiments

We conducted experiments on the three tasks illustrated in Figure 1, also described in Section 3.1, based on the publicly available raw data [24, 33, 38]. For each task, we conducted three rounds of experiments and report mean performance and standard errors. Within each round of experiments, by randomly sampling from disjoint subsets of the raw data (i.e., with *non-overlapping* query classes, cf., Section 3.1), we constructed a different set of train, validation, and test data respectively. Note that only the test dataset includes the key instances’ ID, for evaluating quality of the explanations. In all tables, the best performance is indicated in bold. Appendix B has details on the raw data, feature extractors [14, 19, 28, 31], and training process used in each task.

6.1 Results for QMNIST handwriting verification

We first consider classification performance and quality of the explanations using training datasets with a fixed sample size and without controlling bag sizes, and then go on to consider the effect of varying training sample size and (controlled) average bag sizes.

6.1.1 Classification performance and quality of the explanations

Table 1 reports the classification performance of all methods, including the two non-attention-based ones (MI-Net and Bi-LSTM), on QMNIST using AUROC, accuracy, precision, recall, and F1-score.⁷ It shows the baseline outperforms the benchmark models, while the CAP-based models improve on the baseline and benchmarks in all measures, with statistical significance (at $\geq 95\%$ confidence level) and by substantial margins.

To better understand the exemplar-level verification performance in Table 1, it is worth noting that even though MNIST is generally regarded as a simple dataset, the MI verification task based on it can be highly challenging. To put it in context, for the well-known task of image classification to recognize MNIST digits, usually deemed as a “solved” problem in the literature, a ResNet-18 model can typically achieve above 95% classification accuracy [13]. In contrast, the accuracy of all models in Table 1, using ResNet-18 as a feature extractor, is below 70% on the MI verification task. In addition, our experimental design, constructing each exemplar using the same digit, enables us to break down

⁷We use the macro average for precision, recall, and F1-score because either class may be of interest, e.g., the exemplar label 0 when models are used for anomaly detection, and the label 1 for verification purposes.

Table 1: QMNIST: classification performance (mean and standard errors), including two non-attention-based benchmarks (MI-Net and Bi-LSTM). The best performance is shown in bold.

	AUROC	Accuracy	Precision	Recall	F1-score
Baseline	0.708±0.006	0.658±0.003	0.647±0.003	0.637±0.003	0.637±0.003
GABMIL	0.660±0.017	0.623±0.011	0.613±0.009	0.613±0.009	0.613±0.009
PMA	0.641±0.005	0.604±0.010	0.600±0.006	0.600±0.006	0.597±0.009
MSA	0.634±0.008	0.596±0.004	0.593±0.007	0.597±0.003	0.590±0.006
MI-Net	0.637±0.006	0.593±0.005	0.597±0.003	0.597±0.003	0.593±0.003
Bi-LSTM	0.630±0.005	0.594±0.010	0.590±0.006	0.590±0.006	0.587±0.009
CAP-VEMA(ours)	0.736±0.004	0.675±0.007	0.663±0.007	0.667±0.009	0.667±0.009
CAP-DBA(ours)	0.731±0.011	0.675±0.009	0.667±0.007	0.667±0.007	0.667±0.007

Table 2: Classification performance of CAP-VEMA model on a test QMNIST dataset broken down by digits

Digit	TP ¹	TN ¹	FP ¹	FN ¹	Accuracy (=TP+TN)
“0”	0.246	0.439	0.148	0.167	0.685
“1”	0.282	0.369	0.191	0.158	0.651
“2”	0.266	0.451	0.137	0.146	0.717
“3”	0.231	0.445	0.142	0.182	0.676
“4”	0.259	0.421	0.162	0.158	0.681
“5”	0.261	0.422	0.161	0.156	0.683
“6”	0.318	0.395	0.184	0.103	0.713
“7”	0.292	0.412	0.158	0.138	0.704
“8”	0.238	0.417	0.170	0.175	0.655
“9”	0.273	0.385	0.190	0.152	0.658

¹ TP: True Positive; TN: True Negative; FP: False Positive; FN: False Negative. All figures are relative rate over total number of samples for a specific digit.

Table 3: QMNIST: evaluating quality of the explanations (mean and standard errors). The best performance is shown in bold.

	Avg. i-AUROC	Avg. i-AP
Baseline	0.696 ± 0.001	0.619 ± 0.003
GABMIL	0.506 ± 0.001	0.479 ± 0.002
PMA	0.509 ± 0.004	0.487 ± 0.004
CAP-VEMA	0.832 ± 0.005	0.784 ± 0.007
CAP-DBA	0.825 ± 0.006	0.771 ± 0.005

Average number of instances per bag	Number of key instances			$\left(\frac{\text{Number of key instances}}{\text{Number of instances}}\right)$		
	Mean	Median	Maximum	Mean	Median	Maximum
10	2.742	3.0	8	0.288	0.273	0.8
20	3.699	4.0	15	0.187	0.182	0.682
50	3.273	3.0	10	0.066	0.061	0.222

Table 4: Statistics of “Number of key instances” and “Ratio of (Number of key instances / Number of instances)” with, on average, 10, 20, and 50 instances per target bag.

performance by digits, as shown in Table 2, which facilitates understanding and disentangling relevant factors. Table 2 has performance per digit evaluated using the CAP-VEMA model based on one representative test dataset of this task.

We offer some intuition about why the MNIST MI-verification task can be difficult and draw some observations from Table 2. Intuitively, the high achievable accuracy, and thus easiness, of the digit recognition task demonstrates that the writing styles of different writers are generally consistent—otherwise inconsistent or ambiguous writing patterns would have made it much more difficult to recognize, or differentiate between, digits [25, 26]. Nonetheless, such consistency of writing styles is in fact a major source of difficulty for a verification task, because the goal of verification is to tell apart different writers’ handwriting based on variations in writing style.⁸ MI verification adds further challenge by introducing bags of different writers’ handwriting. This exacerbates the issue of less variation in writing styles since only one confounding writer in a bag can result in the signal being overwhelmed by the noise. Table 2 demonstrates some supporting evidence for this intuition: the digits usually written in a uniform pattern, like “1” and “8”, are more difficult for MI verification, leading to higher false positive/negative rates and thus worse accuracy. Conversely, digits that can be naturally written in diverse ways, such as “2” and “7”, can be more accurately verified.

To enable evaluation of explanation quality, Table 3 shows average i-AUROC and i-AP for the baseline, two benchmarks, and our models. CAP-based models outperform the other three by even larger margins than in the case of classification performance, indicating a superior ability to identify key instances. Notably, the two benchmarks produce significantly worse explanation quality than the baseline, supporting the hypothesis that failure of their attention mechanism to incorporate the query diminishes their ability to accurately model verification tasks of this type.

6.1.2 Effects of training sample size and bag size

Similar to [17], we vary the number of training exemplars and the number of instances per target bag in the training data, and study the effect on model performance. More specifically, we consider mean bag sizes of 10, 20, and 50, with variance 2, 4, and 10, respectively. For mean bag size 10, Figures 5 shows classification performance (AUROC, accuracy) and quality of explanations (average i-AUROC, average i-AP), obtained by varying the number of training exemplars from 8,000 to 40,000. The results for mean bag sizes 20 and 50 can be found in Appendix C, Figures 7 and 8, and are very similar.

Based on these results, it is clear that CAP-based models perform substantially better than the other models, for small and large numbers of training examples. The improvement in quality of the explanations (*cf.* Figure 5b and 5d) is consistent with the hypothesis that this is the main driver for the improvement in classification performance. For average target bag sizes of 20 and 50 instances, similar to the case of bag size 10, our models still significantly outperform other models by substantial margins, according to all criteria.

We also note that all models’ performance deteriorates when the number of instances per target bag increases. A deeper inspection of the data explains the reason. In this task, the source of key instances, *i.e.*, the handwriting of a specific digit from a writer, is limited in the raw data. Because we draw random samples without replacement when generating a bag, key instances in a bag become relatively scarce when we increase the total number of instances in the bag. This can be clearly seen in the second column of Table 4, which presents the mean/median/maximum statistics for the number of key instances per target bag in the training data.

Table 4 shows that when the average bag size increases, the number of key instances per target bag remains stable. Consequently, enlarging the bag size entails adding more non-key instances, or “noise”, to the bag. In other words, the ratio of “Number of key instances / Total number of instances” per bag, akin to a signal-to-noise ratio, decreases with increased bag sizes, see the third column of Table 4. Therefore, in this task, the “number of instances per target bag” effectively becomes a proxy for “noise-to-signal” ratio; the results show that higher noise-to-signal ratio in the training data creates a more difficult verification task, which causes performance deterioration for all models. From Figures 7

⁸In an extreme case, had all writers’ writing style been identical, it would have made the digit recognition task trivial, but made the verification task impossible—that is, no different from random guess—even for humans.

10 instances per target bag on average

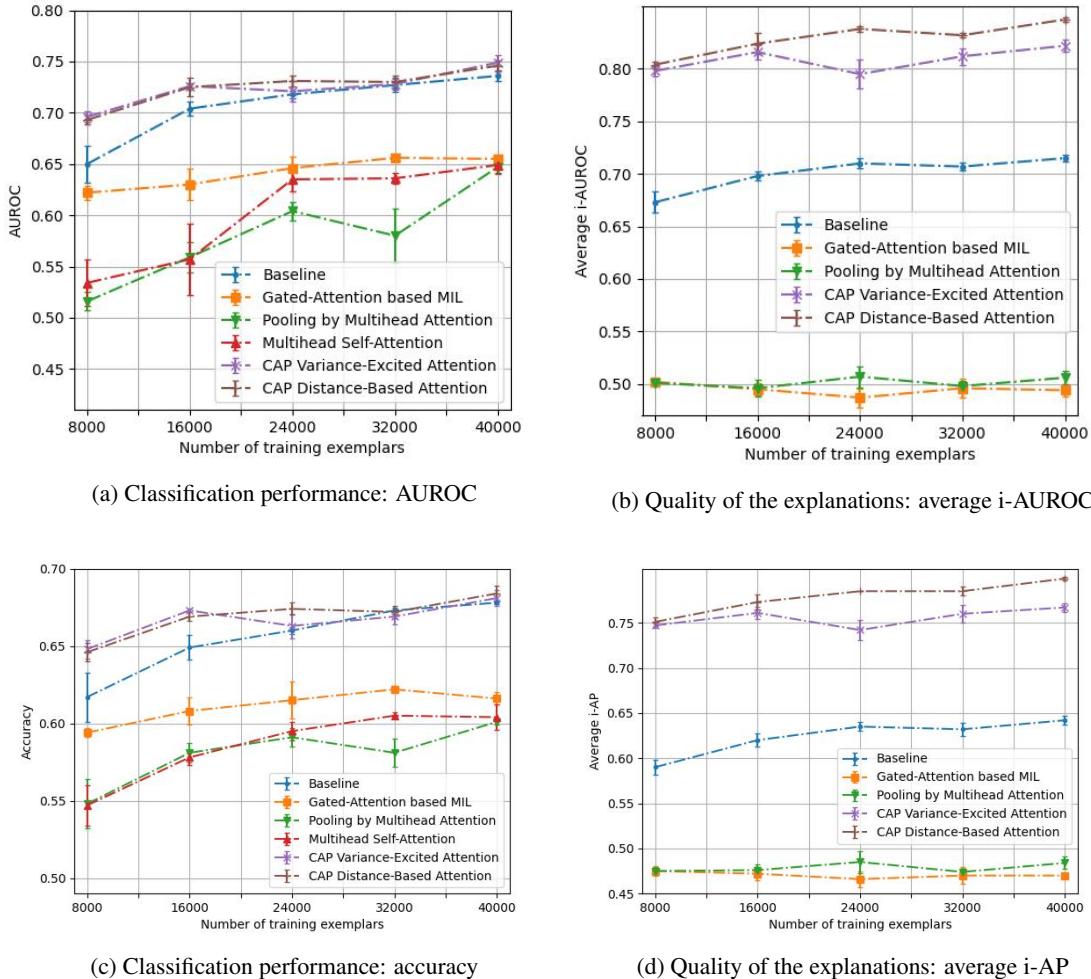


Figure 5: Test AUROC (5a), accuracy (5c), average i-AUROC (5b), average i-AP (5d) for QMNIST when varying numbers of training exemplars, from 8,000 to 40,000, with an average of 10 instances per target bag.

and 8, we also observe that the performance deterioration of our models tends to be less sensitive to the increase of bag size, indicating that our models are more resilient to higher noise-to-signal ratios.

6.2 Results for signature verification against multiple anchors

The main results for signature verification are in Tables 5 and 6, respectively. The CAP-based models consistently exceed the performance of the baseline and benchmarks by sizable margins, according to both predictive performance and explanation quality. In particular, they provide near-perfect explanations, which supports the hypothesis that their superior classification performance is due to their ability to correctly identify instances.

Overall, the pattern of performance in Tables 5 and 6 is similar to that in the first task, with two exceptions. One, our models’ explanation quality is close to perfect whilst their classification accuracy is substantially below 100%. Two, the PMA benchmark appears to perform notably better than the baseline, although with higher standard errors. Considering the first point, as explained in Section 3.1, there are two types of negative exemplars in this task: one has an irrelevant query that is completely different from any anchor; another includes a query that is a professional forgery similar to an (authentic) anchor, sometimes looking even more like the anchors than some truly authentic queries. Because the training data do not disclose what type of query yields a negative exemplar (“irrelevant” or “forgery”)—to mimic the real-world scenarios where the reasons for rejecting a signature are unavailable—solving this task requires essentially a two-step verification process: (1) to identify the correct anchors from a target bag, if they exist; and (2) to verify

Table 5: Signature verification against multiple anchors: classification performance (mean and standard errors), including two non-attention-based benchmarks (MI-Net and Bi-LSTM). The best performance is shown in bold.

	AUROC	Accuracy	Precision	Recall	F1-score
Baseline	0.685±0.014	0.594±0.008	0.697±0.019	0.593±0.009	0.533±0.015
GABMIL	0.688±0.035	0.547±0.018	0.697±0.007	0.547±0.018	0.440±0.036
PMA	0.756±0.031	0.641±0.025	0.687±0.033	0.643±0.023	0.617±0.035
MSA	0.690±0.011	0.619±0.002	0.633±0.003	0.620±0.000	0.610±0.000
MI-Net	0.703±0.039	0.643±0.016	0.673±0.007	0.643±0.017	0.623±0.022
Bi-LSTM	0.733±0.027	0.653±0.019	0.663±0.024	0.653±0.020	0.647±0.018
CAP-VEMA(ours)	0.819±0.006	0.673±0.027	0.733±0.003	0.673±0.029	0.647±0.041
CAP-DBA(ours)	0.814±0.006	0.674±0.018	0.733±0.009	0.673±0.020	0.653±0.029

Table 6: Signature verification against multiple anchors: evaluating the explanations (mean and standard errors). The best performance is shown in bold.

	Avg. i-AUROC	Avg. i-AP
Baseline	0.738 ± 0.021	0.678 ± 0.027
GABMIL	0.533 ± 0.014	0.504 ± 0.006
PMA	0.558 ± 0.011	0.517 ± 0.006
CAP-VEMA	0.995 ± 0.002	0.993 ± 0.003
CAP-DBA	0.993 ± 0.004	0.991 ± 0.005

whether the query is authentic or a forgery when compared to relevant anchors. This process is the same even if humans perform the verification—the first step may be relatively easy while the second can be highly difficult. The near-perfect explanations demonstrate our methods’ ability to perform the first step well while the relatively low accuracy reflects the difficulty of distinguishing between authentic signatures and forgeries in the second step.

Considering PMA’s relatively high classification accuracy, inspection of its explanation quality reveals that correct classifications are often obtained for the wrong reasons—its explanation quality is *far worse* than that of the baseline. This implies that even though some classifications may be “correct”, the *incorrect* key instances in the target bag are chosen when making those classifications. This faulty behaviour is enabled by the fact that PMA uses a trainable seed vector, rather than the query’s feature vector, for MI pooling of the target bag. Intuitively, using incorrect reasoning to obtain classifications implies high variance (standard errors) in classification performance and this is confirmed in Table 5. The discrepancy in average classification performance and explanation quality highlights the importance of assessing both criteria together.

Examples of inconsistency in the accuracy of classifications and quality of the explanations are shown in Figures 6a and 6b. In Figure 6a, there is one key instance: the third instance. Our models correctly identify this key instance with the highest attention score (which is much higher than the second-highest score) and also make the correct classification. The highest attention score of the baseline and GABMIL benchmark does not identify the correct key instance, although the GABMIL’s second-highest score does. Note that both i-AUROC and i-AP correctly reflect GABMIL’s better quality of the explanations than the baseline’s. In both cases, they make an incorrect classification, as expected. The PMA benchmark has the poorest quality of explanations, as expected, because its *lowest* attention score corresponds to the actual key instance. Surprisingly, it makes the correct classification with a high predicted probability.

For the exemplar in Figure 6b, there are two key instances. Our models correctly identify them with the two highest attention scores. Nonetheless, the DBA method makes an incorrect classification, despite the good quality of the explanations. Likewise, the baseline correctly identifies one key instance yet still makes an incorrect classification. Both benchmarks, GABMIL and PMA, are unable to identify the correct key instances, with the two *lowest* attention scores corresponding to the ground truth. Whilst GABMIL makes an incorrect classification as expected, interestingly PMA still makes the correct classification.

6.3 Results for fact extraction and verification

Performance on the FEVER task is shown in Tables 7 and 8. As in the other tasks, CAP-based models outperform the baseline and benchmarks, with statistical significance and by sizable margins—particularly large margins in the quality of explanations. Interestingly, DBA provides slight but consistent improvements over VEMA across all measures.

Query Target: A bag of signatures from numerous writers

					i-AUROC	i-AP	Predicted Probability
Ground Truth	0	0	1	0			
Attention Scores							
Baseline	0	0	0	1	0.333	0.25	0.031
GABMIL	0.233	0.201	0.276	0.29	0.667	0.5	0.005
PMA	0.288	0.107	0.012	0.593	0	0.25	0.987
CAP-VEMA (ours)	0.13	0.041	0.827	0.002	1	1	0.999
CAP-DBA (ours)	0.005	0.005	0.985	0.005	1	1	0.871

(a)

Query Target: A bag of signatures from numerous writers

					i-AUROC	i-AP	Predicted Probability
Ground Truth	1	1	0	0			
Attention Scores							
Baseline	0	1	0	0	0.75	0.75	0.006
GABMIL	0.121	0.149	0.456	0.274	0	0.417	3e-6
PMA	0.041	0.148	0.631	0.18	0	0.417	0.782
CAP-VEMA (ours)	0.543	0.334	0.075	0.048	1	1	0.967
CAP-DBA (ours)	0.638	0.324	0.016	0.022	1	1	0.028

(b)

Figure 6: More examples to illustrate quantitative evaluations of explanations vs. classification. The column “Predicted Probability” shows a model’s predicted probability of the exemplar label. If it is ≥ 0.5 , this exemplar is classified as 1, otherwise 0. Ground-truth of a key instance is highlighted by a red rectangle. Signature images are blurred for data use compliance.

Table 7: Fact extraction and verification (FEVER): classification performance (mean and standard errors), including two non-attention-based benchmarks (MI-Net and Bi-LSTM). The best performance is shown in bold.

	AUROC	Accuracy	Precision	Recall	F1-score
Baseline	0.864±0.004	0.778±0.003	0.780±0.000	0.777±0.003	0.777±0.003
GABMIL	0.864±0.003	0.777±0.002	0.780±0.000	0.777±0.003	0.777±0.003
PMA	0.855±0.002	0.770±0.002	0.773±0.003	0.770±0.000	0.770±0.000
MSA	0.857±0.001	0.771±0.003	0.767±0.003	0.767±0.003	0.767±0.003
MI-Net	0.857±0.002	0.769±0.002	0.770±0.000	0.770±0.000	0.770±0.000
Bi-LSTM	0.860±0.002	0.771±0.001	0.770±0.000	0.770±0.000	0.770±0.000
CAP-VEMA(ours)	0.886±0.002	0.807±0.003	0.813±0.003	0.807±0.003	0.807±0.003
CAP-DBA(ours)	0.898±0.001	0.817±0.003	0.827±0.003	0.817±0.003	0.817±0.003

Table 8: Fact extraction and verification (FEVER): evaluating the explanations (mean and standard errors). The best performance is shown in bold.

	Avg. i-AUROC	Avg. i-AP
Baseline	0.584 ± 0.035	0.384 ± 0.050
GABMIL	0.644 ± 0.013	0.461 ± 0.017
PMA	0.620 ± 0.012	0.444 ± 0.009
CAP-VEMA	0.835 ± 0.001	0.719 ± 0.002
CAP-DBA	0.851 ± 0.004	0.743 ± 0.005

Model Components	Classification		Quality of the explanations	
	AUROC	Accuracy	Avg. i-AUROC	Avg. i-AP
<i>Baseline</i>	<i>0.708</i>	<i>0.658</i>	<i>0.696</i>	<i>0.619</i>
+ New functional form of attention	+0.025	+0.016	+0.135	+0.160
+ Multi-head linear projection	+0.000	+0.004	-0.003	-0.005
+ Squeeze and co-excitation	+0.011	+0.007	-0.019	-0.017
+ Pre-aggregation LayerNorm	-0.008	-0.009	+0.023	+0.028
<i>CAP-VEMA</i>	<i>0.736</i>	<i>0.675</i>	<i>0.832</i>	<i>0.784</i>

(a) Building CAP-VEMA from the baseline.

Model Components	Classification		Quality of the explanations	
	AUROC	Accuracy	Avg. i-AUROC	Avg. i-AP
<i>Baseline</i>	<i>0.708</i>	<i>0.658</i>	<i>0.696</i>	<i>0.619</i>
+ New functional form of attention	+0.009	+0.005	+0.124	+0.147
+ Multi-head linear projection	+0.015	+0.014	+0.008	+0.010
+ Squeeze and co-excitation	+0.004	-0.004	+0.004	+0.009
+ Pre-aggregation LayerNorm	-0.005	+0.002	-0.008	-0.014
<i>CAP-DBA</i>	<i>0.731</i>	<i>0.675</i>	<i>0.825</i>	<i>0.771</i>

(b) Building CAP-DBA from the baseline.

Table 9: Incremental effects of model components by progressively building CAP-VEMA and CAP-DBA from the baseline, in the QMNIST task.

Similar to the second task, there is some inconsistency between the quality of classifications and explanations when comparing the benchmarks to the baseline.

6.4 Ablation study

To understand the effects of components from our models, it is instructive to consider the incremental effects of progressively adding CAP components to the baseline, one component at a time, using both VEMA and DBA attention functions. The results of the incremental effects on performance are presented in Tables 9, 10, 11, for the three tasks respectively.

The QMNIST task is synthesized by generating each exemplar using the same digit, making instances within a target bag all look alike. As such, it may be a well-controlled test of the effectiveness of our approach. Table 9 demonstrates that the new functional forms of attention, VEMA and DBA, contribute far more to quality of explanations than the other components, and a large portion of the classification enhancement. Note that in this task, the baseline’s performance already significantly exceeds that of the three benchmarks (*cf.* Table 1 and 3), possibly due to its attention incorporating the query instance to some extent. Yet on top of the baseline’s performance, VEMA/DBA continue to bring substantial improvement. This strongly supports the effectiveness of our proposed attention functions to tackle the challenges brought by this task. Particularly for DBA, despite its simpler form, we note that its performance is comparable to that of VEMA.

For the two other tasks, signature verification and FEVER, the overall patterns are similar: the new attention functions in conjunction with “squeeze and co-excitation” (SCE) contribute the most to model performance, for both classification and quality of explanations. Again, the functional form of attention contributes the most by far. They and SCE are typically the top two contributors to classification performance.

Model Components	Classification		Quality of the explanations	
	AUROC	Accuracy	Avg. i-AUROC	Avg. i-AP
<i>Baseline</i>	<i>0.685</i>	<i>0.594</i>	<i>0.738</i>	<i>0.678</i>
+ New functional form of attention	+0.047	+0.012	+0.228	+0.277
+ Multi-head linear projection	+0.036	+0.003	+0.018	+0.024
+ Squeeze and co-excitation	+0.043	+0.053	+0.007	+0.009
+ Pre-aggregation LayerNorm	+0.008	+0.011	+0.005	+0.006
<i>CAP-VEMA</i>	<i>0.819</i>	<i>0.673</i>	<i>0.995</i>	<i>0.993</i>

(a) Building CAP-VEMA from the baseline.

Model Components	Classification		Quality of the explanations	
	AUROC	Accuracy	Avg. i-AUROC	Avg. i-AP
<i>Baseline</i>	<i>0.685</i>	<i>0.594</i>	<i>0.738</i>	<i>0.678</i>
+ New functional form of attention	+0.064	+0.013	+0.243	+0.299
+ Multi-head linear projection	-0.023	+0.011	+0.005	+0.006
+ Squeeze and co-excitation	+0.073	+0.045	+0.006	+0.007
+ Pre-aggregation LayerNorm	+0.015	+0.011	+0.001	+0.001
<i>CAP-DBA</i>	<i>0.814</i>	<i>0.674</i>	<i>0.993</i>	<i>0.991</i>

(b) Building CAP-DBA from the baseline.

Table 10: Incremental effects of model components by progressively building CAP-VEMA and CAP-DBA from the baseline, in the signature verification task.

Model Components	Classification		Quality of the explanations	
	AUROC	Accuracy	Avg. i-AUROC	Avg. i-AP
<i>Baseline</i>	<i>0.864</i>	<i>0.778</i>	<i>0.584</i>	<i>0.384</i>
+ New functional form of attention	+0.011	+0.017	+0.185	+0.254
+ Multi-head linear projection	+0.003	+0.004	+0.039	+0.040
+ Squeeze and co-excitation	+0.010	+0.008	+0.008	+0.012
+ Pre-aggregation LayerNorm	-0.002	+0.000	+0.020	+0.029
<i>CAP-VEMA</i>	<i>0.886</i>	<i>0.807</i>	<i>0.835</i>	<i>0.719</i>

(a) Building CAP-VEMA from the baseline.

Model Components	Classification		Quality of the explanations	
	AUROC	Accuracy	Avg. i-AUROC	Avg. i-AP
<i>Baseline</i>	<i>0.864</i>	<i>0.778</i>	<i>0.584</i>	<i>0.384</i>
+ New functional form of attention	+0.018	+0.022	+0.206	+0.281
+ Multi-head linear projection	+0.001	+0.005	+0.038	+0.046
+ Squeeze and co-excitation	+0.010	+0.010	-0.016	-0.018
+ Pre-aggregation LayerNorm	+0.006	+0.003	+0.039	+0.050
<i>CAP-DBA</i>	<i>0.898</i>	<i>0.817</i>	<i>0.851</i>	<i>0.743</i>

(b) Building CAP-DBA from the baseline.

Table 11: Incremental effects of model components by progressively building CAP-VEMA and CAP-DBA from the baseline, in the FEVER task.

Results demonstrate that the majority of uplift in capability to identify key instances can be attributed to the new functional forms of attention, VEMA and DBA. In conjunction with SCE, they also contribute the most to classification enhancement.

On the other hand, the contribution of the multi-head projection is mixed. When moving from the “non-headed” version (without linear projections) to a multi-head version, the performance differences vary across tasks and measures. Additional analyses provided in Appendix D isolate effects from the multi-head mechanism by comparing models with and without multiple heads. Those analyses demonstrate the limited contribution from the multi-head mechanism, consistent with the results in this section. The reason may be that, in these tasks, each instance is typically an independent and complete object with a holistic—not partial—feature representation, while the multi-head mechanism is designed “to jointly attend to information from different *representation subspaces* at different positions” [34]. Therefore, given the presence of other model components, multi-headedness alone appears to add little value in the tasks considered in this paper.⁹

Finally, from Tables 10 and 11 we observe that there are consistent improvements brought by the component of multi-head “pre-aggregation LayerNorm” (*cf.* Equations (8a), (8b), as the last element in the CAP architecture), compared to no normalization. To check the robustness of CAP to such normalization, we tested the sensitivity of our model results to an alternative form of LayerNorm, shown in Appendix E. This alternative is a standard LayerNorm without multi-headness, akin to the post-attention LayerNorm adopted in the transformer model, applied *after* bag aggregation and *after* all heads are concatenated in Equations (8a) and (8b). Henceforth, we call it “post-aggregation LayerNorm”. The results in Appendix E show similar performance of CAP-based models when the pre-aggregation LayerNorm is replaced with the post-aggregation LayerNorm, and thus demonstrate the robustness of CAP to different forms of output normalization.

7 Conclusions and future research

We introduce MI verification, which combines verification and MIL, and show theoretically and empirically that a lack of information about the query instance in attention is undesirable when pooling the target bag into a bag-level representation. To empirically demonstrate this, we construct a simple baseline model and three benchmark models, adapted from SOTA attention-based MIL methods, that omit the query in attention, and create a new approach named “Cross Attention Pooling” (CAP) that explicitly considers the query in attention, along with two new attention functions within the CAP framework. Results on three different tasks show that the benchmark methods are not better, and sometimes significantly worse, than the simple baseline. In contrast, the CAP-based methods outperform the baseline and benchmarks by sizeable margins in terms of both classification and quality of explanations. Ablation studies confirm the superior ability of the new attention functions to identify key instances and establish the contributions of the key components of the CAP architecture.

The abstract representation of “MI verification”, as distinct from traditional MIL opens up the potential for research on a broad range of problems and applications. For example, either the “query” or the “target” may be a single instance, bag of instances, or bag of bags, and they may exhibit different modalities—for example, one may be textual and the other may consist of images. We believe our work provides a generic framework that may inspire research in directions such as new architectures, attention mechanisms, real-world applications, and methods for generating explanations and evaluating their quality.

As a first step towards tackling MI verification, our paper also offers future opportunities connecting to some domain-specific, well-established research areas. For example, while this paper considers CV datasets that enable well-controlled experiments and disentangling factors without compromising on the difficulty of tasks, applications of MI verification on more complex datasets such as ImageNet or MS-COCO may lead to research of weakly-supervised one-shot object detection or weakly-supervised cross-domain retrieval (*cf.* Section 3). For the NLP domain, a comparison of our approach to other methods specifically designed for particular tasks, e.g., FEVER, may also be an interesting topic for prospective research (*cf.* Section 2). Interpretability of weakly supervised learning and its evaluation is yet another avenue that this work can be extended to. Those research topics are sufficiently significant and challenging to warrant dedicated, standalone future studies.

⁹Note that the transformer used separate multi-head projections for each “query, key, value” triplet in attention. Based on the ablation results, we chose not to use separate projections for our experiments. Instead, we opted for less model complexity, by employing a single, shared linear projection in the multi-head formulation of CAP.

Appendices

A Proof of Proposition 1

Proof. [Proposition 1: Variables incorporated in the attention scores]

Because it is well-known that

$$H(U | V^{Target}) \geq H(U | V^{Query}, V^{Target}),$$

that is, adding more conditioning variables cannot decrease informativeness, to prove Inequality (4), we only need to show $H(U | V^{Target}) \neq H(U | V^{Query}, V^{Target})$. We prove this by contradiction.

Based on the well-known property of conditional entropy and mutual information,

$$H(U | V^{Query}, V^{Target}) = H(U | V^{Target}) - I(U, V^{Query} | V^{Target}), \quad (11)$$

where $I(\cdot, \cdot | \cdot)$ denotes the conditional mutual information. It has the well-known non-negativity property, $I \geq 0$, if all random variables are valued in standard Borel spaces.

By symmetry, we can also obtain the following equation analogous to (11):

$$H(U | V^{Query}, V^{Target}) = H(U | V^{Query}) - I(U, V^{Target} | V^{Query}). \quad (12)$$

Subtracting Equation (12) from Equation (11) and re-arranging, we get

$$H(U | V^{Target}) - I(U, V^{Query} | V^{Target}) = H(U | V^{Query}) - I(U, V^{Target} | V^{Query}). \quad (13)$$

Now, if $H(U | V^{Target}) = H(U | V^{Query}, V^{Target})$, based on Equation (11), $I(U, V^{Query} | V^{Target}) = 0$, and thus Equation (13) becomes

$$\begin{aligned} H(U | V^{Target}) &= H(U | V^{Query}) - I(U, V^{Target} | V^{Query}) \implies \\ H(U | V^{Target}) &\leq H(U | V^{Query}) \quad (\text{Non-negativity of } I(U, V^{Target} | V^{Query})). \end{aligned} \quad (14)$$

As a result, Inequality (14) must always hold, for all values of V^{Target} , V^{Query} , implying

$$Pr(H(U | V^{Target}) > H(U | V^{Query})) = 0,$$

which contradicts Assumption 1 because the assumption requires

$$Pr(H(U | V^{Target}) > H(U | V^{Query})) > 0.$$

This concludes the proof of Inequality (4). By symmetry, Inequality (5) can also be shown in a similar manner, which completes the proof of Proposition 1. \square

B Details of data and training process

The following details of training are common to all three tasks considered in the experiments.

Prior to full training of all network parameters, we adopt an initial learning stage where we freeze the feature extractor’s model weights and train only the parameters specific to the baseline, benchmarks. This initial phase is stopped when the accuracy on the validation dataset does not improve for two epochs.

Subsequently, when all parameters are trained end-to-end, we also adopt early stopping based on validation accuracy, with different stopping criteria for different tasks as discussed below. The optimization for training is conducted using the RMSprop optimizer, with the same parameters for all models: $\rho = 0.9$, $\epsilon = 1e-7$. Due to a well-known behavior of “batch normalization” (BatchNorm) causing degradation in performance during transfer learning [19], we freeze the BatchNorm layers, if any, in a feature extractor, typically for CV tasks. More precisely, the BatchNorm moving average and the trainable parameters are not updated during training.¹⁰

¹⁰We also tried allowing parameters to be trainable but not updating the moving average parameters and found similar experimental results.

For each task, we conducted three rounds of experiments for all models considered in this paper. All experiments were run on a cluster of four NVIDIA RTX A6000 GPUs, of which the duration varies depending on early stopping triggers. Roughly speaking, a single round of training of one model takes approximately one hour for the QMNIST task, two to three hours for the FEVER task, and three to five hours for the signature verification task.

All models were developed using Tensorflow 2.9.3, with some use of “TensorFlow official models” 2.9.0 [40] (Apache License 2.0) and scikit-learn 1.2.0 [27] (BSD License). The original license/terms-of-use of the assets (i.e., raw data, pre-trained feature extractors) used in our research are listed alongside each asset mentioned below.

B.1 QMNIST handwriting verification

We collected QMNIST data (BSD-style license, <https://github.com/facebookresearch/qmnist/blob/main/LICENSE>) according to [38] and from links therein. QMNIST was created to be similar in structure to MNIST, with a training set composed of 60,000 images of digits (“Train/60K”) and a test set of 10,000 digits (“Test/10K”). These two sets turn out to have non-overlapping writer-IDs, which is ideal for our requirement that test writer’s handwriting is not seen during training. We constructed a training dataset by randomly selecting from the “Train/60K” set, including both the query and target bag. To construct the validation and test datasets, we first split “Test/10K” into two sets with non-overlapping writer-IDs and then drew random samples from each set. By construction, the sample sizes of the train/dev/test datasets are 21,509/2,408/2,253 respectively (the same sample sizes for all rounds of experiments were used to draw random samples), and the proportions of their exemplar labels are approximately 50:50. In an exemplar, the bag size N varies between 3 and 25, with a mean of 6.9 instances per target bag and a variance of 6.4 approximately.

We employed ResNet-18 [14] as the feature extractor, initialized by a set of pre-trained weights based on ImageNet. The pre-trained weights were downloaded from <https://pypi.org/project/image-classifiers> (MIT License). Prior to inputting the QMNIST images into ResNet-18, we resized them from their original size of (28×28) to (32×32) , because this is the minimum input size required by ResNet-18. After putting an image through ResNet-18, we obtained its feature vector by applying a “Global Average Pooling” (GAP) on the output of the feature extractor’s penultimate layer.

The learning rate of the RMSprop optimizer was piece-wise constant: $1e-4$ for the first 5 epochs, $5e-5$ for the next 15 epochs, and $2e-5$ for the remaining epochs. The mini-batch size was 768, and the early-stopping criterion was non-improving validation accuracy for 30 epochs. The number of heads was two for any verification models that support multi-head attention.

B.2 Signature verification against multiple anchors

We collected raw images of signatures, both authentic and forged, based on [24] and from the link [http://www.iapr-tc11.org/mediawiki/index.php/ICDAR_2011_Signature_Verification_Competition_\(SigComp2011\)](http://www.iapr-tc11.org/mediawiki/index.php/ICDAR_2011_Signature_Verification_Competition_(SigComp2011)) (data disclaimer: http://www.iapr-tc11.org/dataset/ICDAR_SignatureVerification/SigComp2011/disclaimer.pdf). We resized all signature images from their original sizes to (512×256) and converted them from RGB to black-and-white. To construct the train, validation, and test datasets for each round of the experiment, we first split the raw data into three sets with non-overlapping writer-IDs and then drew random samples from each set. The sample size for training is around 82,000, and for validation/test is close to 10,000. By construction, the proportion of exemplar labels in all datasets is approximately 50:50. In an exemplar, the bag size N varies between two and eight.

For the feature extractor, we employed one from the EfficientNetV2 family [31], called “EfficientNetV2B3”, initialized with ImageNet-pretrained weights. The pretrained weights were downloaded from https://www.tensorflow.org/versions/r2.9/api_docs/python/tf/keras/applications/efficientnet_v2/EfficientNetV2B3 (CC-BY-4.0 license). We resized all the signature images to an identical size of (256×128) . After putting an image through EfficientNetV2B3, we obtained its feature vector by applying global average pooling on the output from the penultimate layer.

The learning rate of the RMSprop optimizer was piece-wise constant: $5e-6$ for the first 5 epochs, $2e-6$ for the next 5 epochs, and $1e-6$ for the remaining epochs. The mini-batch size was 64, and the early-stopping criterion for training was non-improving validation accuracy for 10 epochs. The number of heads was set to six for multi-head attention.

B.3 Fact extraction and verification

For “fact extraction and verification” (FEVER), we collected the raw data of claims and evidence as in [33] and from the FEVER (2018) website <https://fever.ai/dataset/fever.html> (license see <https://fever.ai/download/fever/license.html>). The FEVER raw data was already split into training, validation, and test data, based on a pre-processed dump (June 2017) of Wikipedia pages—more precisely, the corresponding links are: <https://fever.ai/download/fever/train.jsonl>, https://fever.ai/download/fever/paper_dev.jsonl, https://fever.ai/download/fever/paper_test.jsonl, <https://fever.ai/download/fever/wiki-pages.zip>. For all three rounds of experiments, we used the full set of raw validation/test data (6616/6613 exemplars respectively) as our validation/test datasets. To construct our training dataset in each round of experiments, we randomly sampled 33,000 exemplars from the raw training set, with the proportion of the exemplar labels being

20 instances per target bag on average

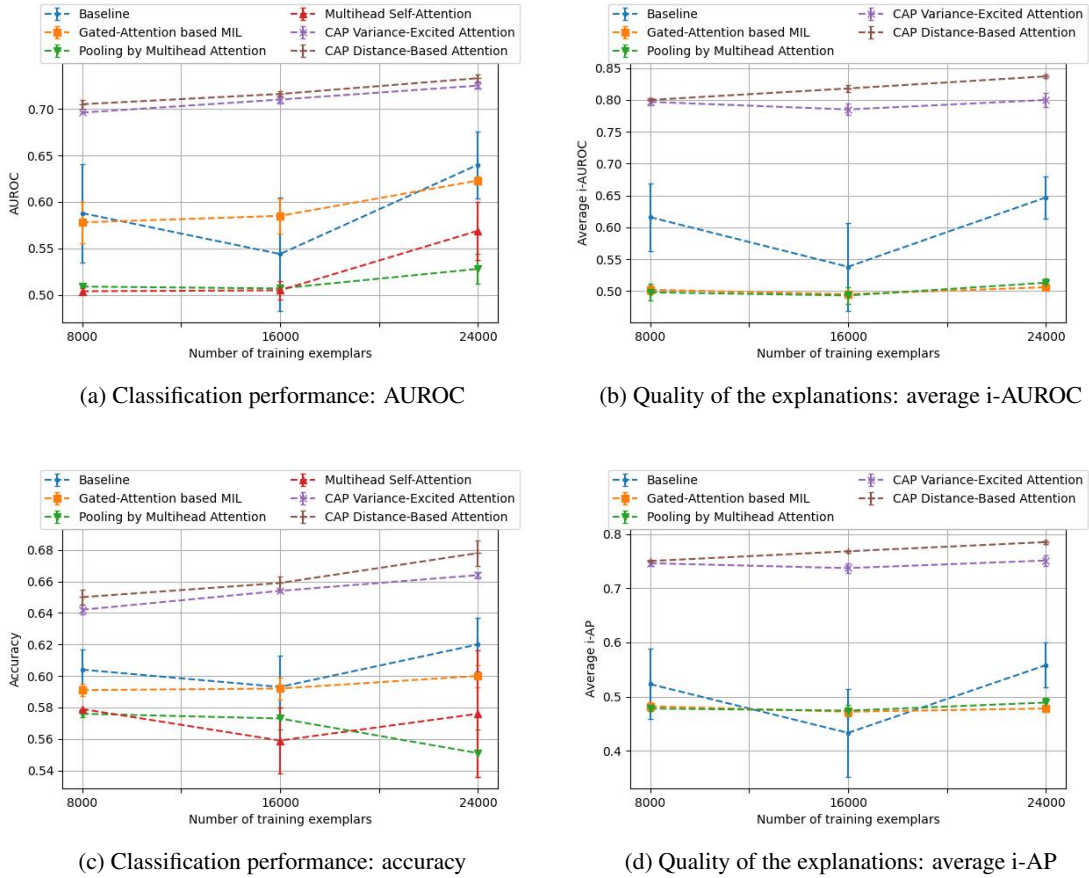


Figure 7: Test AUROC (7a), accuracy (7c), average i-AUROC (7b), average i-AP (7d) for QMNIST for varying numbers of training exemplars, from 8,000 to 24,000, with an average of 20 instances per target bag.

approximately 50:50. In an exemplar, we truncated the amount of evidence in a bag, i.e., the bag size N , if it was greater than 47, and capped the number of tokens in a piece of evidence to 96.¹¹

For the feature extractor, we employed one from the Sentence-BERT (SBERT) family [28], called “multi-qa-MiniLM-L6-cos-v1”, initialized with weights pretrained based on 215M question-answer pairs from various sources. We also used SBERT’s native tokenizer to pre-process all our datasets. See more details, downloadable weights, and the tokenizer at https://www.sbert.net/docs/pretrained_models.html (Apache License 2.0, <https://github.com/UKPLab/sentence-transformers/blob/master/LICENSE>). We obtained the feature vector of any textual paragraph by putting it through the feature extractor, and retrieved the vector of SBERT’s special token “[CLS]”¹² from the models’ penultimate layer.

The learning rate of the RMSprop optimizer was piece-wise constant: $1e-5$ for the first 10 epochs, $5e-6$ for the next 10 epochs, and $2e-6$ for the remaining epochs. The mini-batch size was 48, and the early-stopping criterion was non-improving validation accuracy for 10 epochs. The number of heads was set to four for multi-head attention.

C QMNIST: Results for larger average bag sizes

Learning curves for the QMNIST data for mean bag sizes 20 and 50 are shown in Figures 7 and 8 respectively, in the range of 8,000 to 24,000 training exemplars.

¹¹The truncations are purely for technical reasons (to limit the use of memory/computing), and we found it impacts less than 10% of the total samples.

¹²Note the vector of SBERT’s special token “[CLS]” is different from that of the MSA benchmark’s “[CLS]”.

50 instances per target bag on average

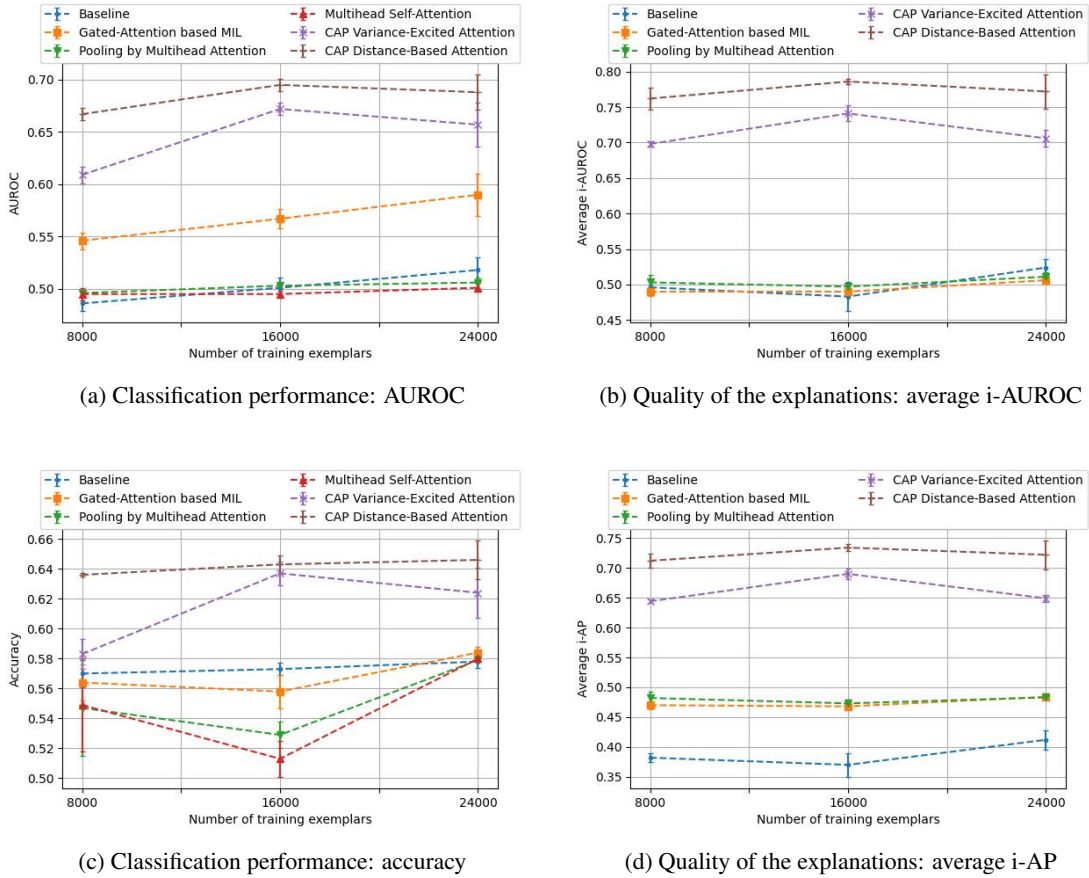


Figure 8: Test AUROC (8a), accuracy (8c), average i-AUROC (8b), average i-AP (8d) for QMNIST for varying numbers of training exemplars, from 8,000 to 24,000, with an average of 50 instances per target bag.

D Does multi-head attention matter?

Given the widespread popularity of multi-head attention in the transformer literature, this section analyzes the contribution of the multi-head projection component, leaving all else intact in CAP. To attribute model performance to the multi-head mechanism, we train models with and without the linear projection to multiple heads. We also refer to attention *without* multi-head projection as “non-headed”.

Figures 9, 10, 11 report the out-of-sample results of the “multi-head” and “non-headed” versions of DBA and VEMA under the CAP framework, on the three tasks respectively.

Generally speaking, the differences between the multi-head and non-headed versions are small, either insignificant or marginally significant. For the CV tasks (QMNIST and signature verification), whilst multi-head VEMA obtains statistically indistinguishable improvements over the non-headed version, CAP-DBA has even slightly better performance by excluding the multi-head projection, albeit with little statistical significance. For the NLP task (FEVER), the results are inconclusive. Even though better quality of explanation is notable for models with multi-head projection, this nevertheless does not translate to better classification—actually, we obtain significantly worse classification performance—for both CAP-VEMA and CAP-DBA (*cf.* Figure 11a).

E Sensitivity of our models to different forms of LayerNorm

One alternative to pre-aggregation LayerNorm is the post-aggregation LayerNorm adopted in the transformer model, i.e. a standard LayerNorm without multi-headedness. We replace the pre-aggregation LayerNorm with this alternative in both CAP-VEMA and CAP-DBA, and compare performance before and after replacement.

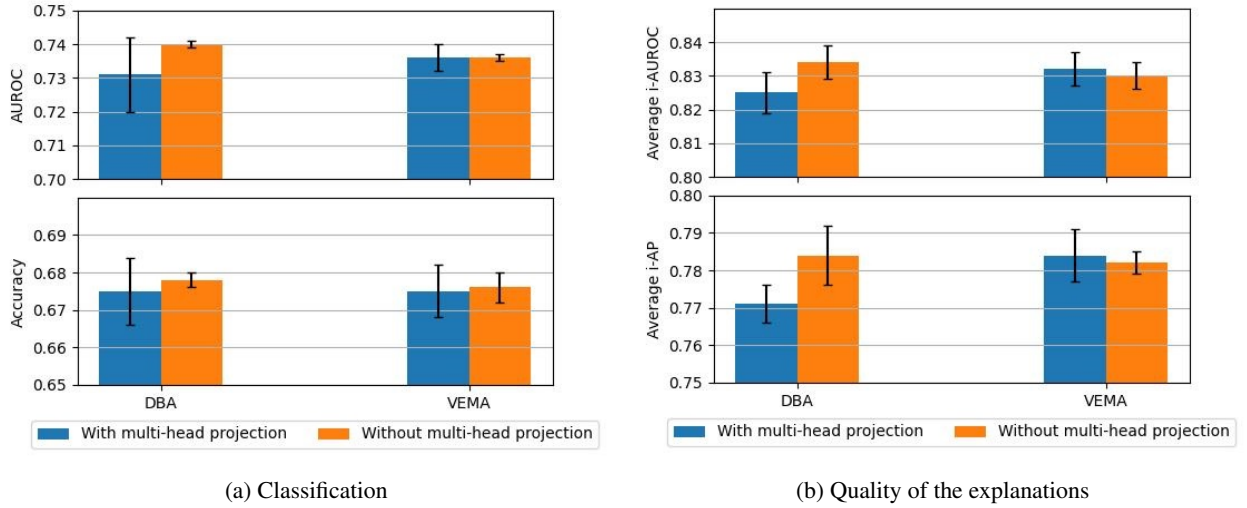


Figure 9: Model performance for the QMNIST task under our CAP framework (DBA and VEMA), with and without the multi-head linear projections. Left column (9a) is classification performance; right column (9b) shows quality of the explanations.

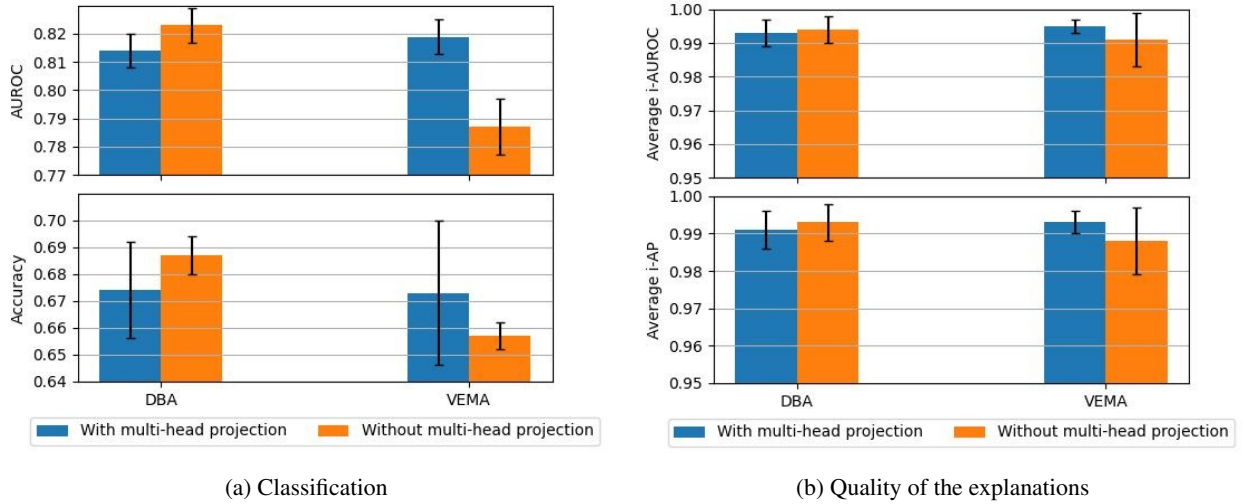


Figure 10: Model performance for the signature verification task under our CAP framework (DBA and VEMA), with and without the multi-head linear projections. Left column (10a) is classification performance; right column (10b) shows quality of the explanations.

Layer Normalization		Classification		Quality of the explanations	
		AUROC	Accuracy	Avg. i-AUROC	Avg. i-AP
CAP-VEMA	Post-aggregation	0.728±0.001	0.672±0.003	0.806±0.020	0.757±0.019
	Pre-aggregation	0.736±0.004	0.675±0.007	0.832±0.005	0.784±0.007
CAP-DBA	Post-aggregation	0.738±0.005	0.684±0.006	0.839±0.004	0.790±0.004
	Pre-aggregation	0.731±0.011	0.675±0.009	0.825±0.006	0.771±0.005

Table 12: Comparisons between pre-aggregation LayerNorm and an alternative of post-aggregation LayerNorm, on the QMNIST handwriting verification task. Higher performance metrics are bolded.

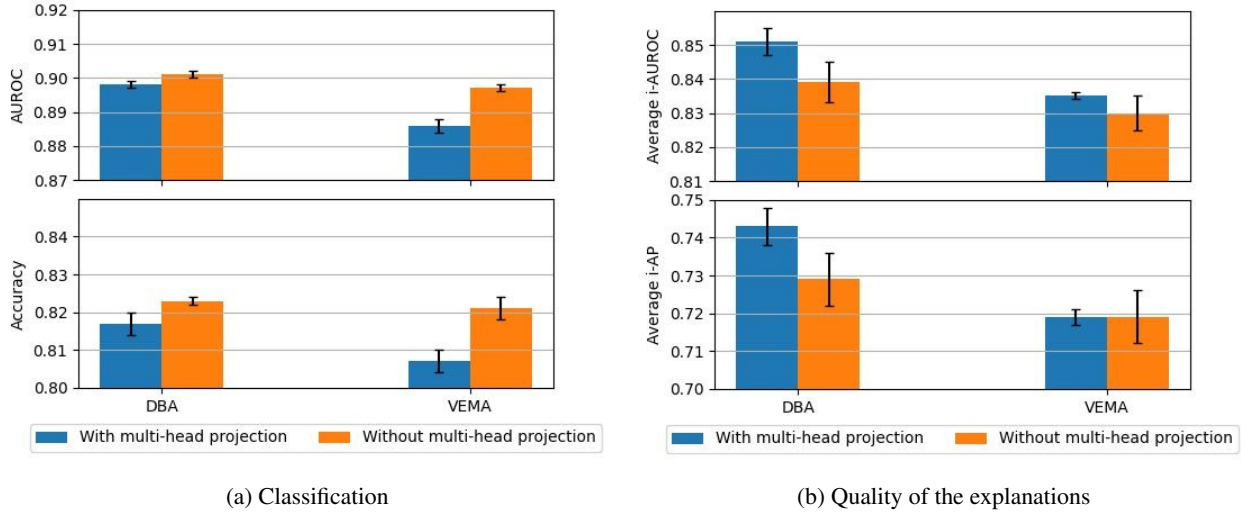


Figure 11: Model performance for the FEVER task under our CAP framework (DBA and VEMA), with and without the multi-head linear projections. Left column (11a) is classification performance; right column (11b) shows quality of the explanations.

Layer Normalization		Classification		Quality of the explanations	
		AUROC	Accuracy	Avg. i-AUROC	Avg. i-AP
<i>CAP-VEMA</i>	Post-aggregation	0.809 ± 0.005	0.669 ± 0.005	0.993 ± 0.004	0.991 ± 0.005
	Pre-aggregation	0.819 ± 0.006	0.673 ± 0.027	0.995 ± 0.002	0.993 ± 0.003
<i>CAP-DBA</i>	Post-aggregation	0.805 ± 0.014	0.660 ± 0.012	0.993 ± 0.005	0.991 ± 0.006
	Pre-aggregation	0.814 ± 0.006	0.674 ± 0.018	0.993 ± 0.004	0.991 ± 0.005

Table 13: Comparisons between pre-aggregation LayerNorm and an alternative of post-aggregation LayerNorm, on the signature verification task. Higher performance metrics are bolded.

Layer Normalization		Classification		Quality of the explanations	
		AUROC	Accuracy	Avg. i-AUROC	Avg. i-AP
<i>CAP-VEMA</i>	Post-aggregation	0.892 ± 0.001	0.811 ± 0.002	0.838 ± 0.001	0.725 ± 0.002
	Pre-aggregation	0.886 ± 0.002	0.807 ± 0.003	0.835 ± 0.001	0.719 ± 0.002
<i>CAP-DBA</i>	Post-aggregation	0.897 ± 0.001	0.818 ± 0.001	0.838 ± 0.006	0.728 ± 0.007
	Pre-aggregation	0.898 ± 0.001	0.817 ± 0.003	0.851 ± 0.004	0.743 ± 0.005

Table 14: Comparisons between pre-aggregation LayerNorm and an alternative of post-aggregation LayerNorm, on the FEVER task. Higher performance metrics are bolded.

The results, shown in Tables 12, 13, 14 for the three tasks respectively, are mixed, across classification performance and quality of the explanations, and across different tasks. The performance differences between the two treatments are generally insignificant or only marginally significant. The results indicate no clear winner and demonstrate that CAP-based models are not sensitive to different forms of LayerNorm when applied in the final step before output. Therefore, their performances are robust to the choices of output normalization.

References

- [1] Jimmy Lei Ba, Jamie Ryan Kiros, and Geoffrey E. Hinton. Layer normalization. *arXiv preprint arXiv:1607.06450*, 2016.
- [2] Jane Bromley, Isabelle Guyon, Yann LeCun, Eduard Säckinger, and Roopak Shah. Signature verification using a “siamese” time delay neural network. In *Advances in Neural Information Processing Systems*, volume 6, 1993.
- [3] Marc-André Carbonneau, Veronika Cheplygina, Eric Granger, and Ghyslain Gagnon. Multiple instance learning: A survey of problem characteristics and applications. *Pattern Recognition*, 77:329–353, 2018.
- [4] Ting Chen, Simon Kornblith, Mohammad Norouzi 0002, and Geoffrey E. Hinton. A simple framework for contrastive learning of visual representations. In *Proceedings of the 37th International Conference on Machine Learning, ICML 2020*, volume 119, pages 1597–1607, 2020.
- [5] Junsuk Choe, Seong Joon Oh, Sanghyuk Chun, Seungho Lee, Zeynep Akata, and Hyunjung Shim. Evaluation for weakly supervised object localization: Protocol, metrics, and datasets. *IEEE Transactions on Pattern Analysis and Machine Intelligence*, 45(2):1732–1748, 2023.
- [6] Sumit Chopra, Raia Hadsell, and Yann LeCun. Learning a similarity metric discriminatively, with application to face verification. In *Proceedings of the 2005 IEEE Computer Society Conference on Computer Vision and Pattern Recognition (CVPR’05)*, volume 1, pages 539–546, 2005.
- [7] Alexis Conneau, Douwe Kiela, Holger Schwenk, Loïc Barrault, and Antoine Bordes. Supervised learning of universal sentence representations from natural language inference data. In *Proceedings of the 2017 Conference on Empirical Methods in Natural Language Processing (EMNLP)*, pages 670–680, 2017.
- [8] Thomas M. Cover and Joy A. Thomas. *Elements of Information Theory 2nd Edition*. Wiley-Interscience, 2006.
- [9] Jesse Davis and Mark Goadrich. The relationship between precision-recall and roc curves. In *Proceedings of the 23rd International Conference on Machine Learning*, volume 06, pages 233–240, 2006.
- [10] Thomas G. Dietterich, Richard H. Lathrop, and Tomás Lozano-Pérez. Solving the multiple instance problem with axis-parallel rectangles. *Artificial Intelligence*, 89(1):31–71, 1997.
- [11] Alexey Dosovitskiy, Lucas Beyer, Alexander Kolesnikov, Dirk Weissenborn, Xiaohua Zhai, Thomas Unterthiner, Mostafa Dehghani, Matthias Minderer, Georg Heigold, Sylvain Gelly, Jakob Uszkoreit, and Neil Houlsby. An image is worth 16x16 words: Transformers for image recognition at scale. In *International Conference on Learning Representations*, 2021.
- [12] Joseph Early, Christine Evers, and Sarvapali Ramchurn. Model agnostic interpretability for multiple instance learning. In *ICLR*, 2022.
- [13] Avrajit Ghosh, He Lyu, Xitong Zhang, and Rongrong Wang. Implicit regularization in heavy-ball momentum accelerated stochastic gradient descent. In *The Eleventh International Conference on Learning Representations (ICLR)*, 2023.
- [14] Kaiming He, Xiangyu Zhang, Shaoqing Ren, and Jian Sun. Deep residual learning for image recognition. In *2016 IEEE Conference on Computer Vision and Pattern Recognition (CVPR)*, pages 770–778, 2016.
- [15] Ting-I Hsieh, Yi-Chen Lo, Hwann-Tzong Chen, and Tyng-Luh Liu. One-shot object detection with co-attention and co-excitation. In *Advances in Neural Information Processing Systems*, 2019.
- [16] Jie Hu, Li Shen, and Gang Sun. Squeeze-and-excitation networks. In *Computer Vision and Pattern Recognition*, pages 7132–7141, 2018.
- [17] Maximilian Ilse, Jakub M. Tomczak, and M. Welling. Attention-based deep multiple instance learning. In *Proceedings of the 35th International Conference on Machine Learning*, pages 2127–2136, 2018.
- [18] Yunzhe Jia, Eibe Frank, Bernhard Pfahringer, Albert Bifet, and Nick Jin Sean Lim. Studying and exploiting the relationship between model accuracy and explanation quality. In *ECML-PKDD*, 2021.
- [19] Fahdi Kanavati and Masayuki Tsuneki. Partial transfusion: on the expressive influence of trainable batch norm parameters for transfer learning. In *Proceedings of Machine Learning Research*, volume 143, pages 338–353, 2021.

- [20] Gregory Koch, Richard Zemel, and Ruslan Salakhutdinov. Siamese neural networks for one-shot image recognition. In *Proceedings of the 32nd International Conference on Machine Learning*, 2015.
- [21] Juho Lee, Yoonho Lee, Jungtaek Kim, Adam R. Kosiorek, Seungjin Choi, and Yee Whye Teh. Set transformer: A framework for attention-based permutation-invariant neural networks. In *Proceedings of the 36th International Conference on Machine Learning*, pages 3744–3753, 2019.
- [22] Weixin Li and Nuno Vasconcelos. Multiple instance learning for soft bags via top instances. In *2015 IEEE Conference on Computer Vision and Pattern Recognition (CVPR)*, pages 4277–4285, 2015.
- [23] Xiaokai Liu, Sheng Bi, Xiaorui Ma, and Jie Wang. Multi-instance convolutional neural network for multi-shot person re-identification. *Neurocomputing*, 337:303–314, 2019.
- [24] Marcus Liwicki, Michael Blumenstein, Elisa van den Heuvel, Charles E.H. Berger, Reinoud D. Stoel, Bryan Found, Xiaohong Chen, and Muhammad Imran Malik. Sigcomp11: Signature verification competition for on- and offline skilled forgeries. In *Proc. 11th Int. Conference on Document analysis and Recognition*, 2011.
- [25] Jishnu Mukhoti, Andreas Kirsch, Joost van Amersfoort, Philip H. S. Torr, and Yarin Gal. Deterministic neural networks with appropriate inductive biases capture epistemic and aleatoric uncertainty. *arXiv preprint arXiv:2102.11582*, 2021.
- [26] Jeongeun Park, Seungyou Shin, Sangheum Hwang, and Sungjoon Choi. Elucidating robust learning with uncertainty-aware corruption pattern estimation. *Pattern Recognition*, 138:109387, 2023.
- [27] F. Pedregosa, G. Varoquaux, A. Gramfort, V. Michel, B. Thirion, O. Grisel, M. Blondel, P. Prettenhofer, R. Weiss, V. Dubourg, J. Vanderplas, A. Passos, D. Cournapeau, M. Brucher, M. Perrot, and E. Duchesnay. Scikit-learn: Machine learning in Python. *Journal of Machine Learning Research*, 12:2825–2830, 2011.
- [28] Nils Reimers and Iryna Gurevych. Sentence-bert: Sentence embeddings using siamese bert-networks. In *EMNLP*, 2019.
- [29] Aalok Sathe and Joonsuk Park. Automatic fact-checking with document-level annotations using BERT and multiple instance learning. In *Proceedings of the Fourth Workshop on Fact Extraction and VERification (FEVER)*, pages 101–107. Association for Computational Linguistics, 2021.
- [30] Zhucheng Shao, Hao Bian, Yang Chen, Yifeng Wang, Jian Zhang, Xiangyang Ji, and Yongbing Zhang. Transmil: Transformer based correlated multiple instance learning for whole slide image classification. In *Advances in Neural Information Processing Systems*, 2021.
- [31] Mingxing Tan and Quoc V. Le. EfficientNetV2: Smaller models and faster training. In *International Conference on Machine Learning*, 2021.
- [32] M. Tarek, E. Hamouda, and A.S. Abohamama. Multi-instance cancellable biometrics schemes based on generative adversarial network. *Applied Intelligence*, 52(1):501–513, 2022.
- [33] James Thorne, Andreas Vlachos, Christos Christodoulopoulos, and Arpit Mittal. FEVER: a large-scale dataset for fact extraction and VERification. In *NAACL-HLT*, 2018.
- [34] Ashish Vaswani, Noam Shazeer, Niki Parmar, Jakob Uszkoreit, Llion Jones, Aidan N. Gomez, Lukasz Kaiser, and Illia Polosukhin. Attention is all you need. In *Advances in Neural Information Processing Systems*, pages 5998–6008, 2017.
- [35] Kaili Wang, José Oramas M., and Tinne Tuytelaars. In defense of LSTMs for addressing multiple instance learning problems. In *15th ACCV*, pages 444–460, 2020.
- [36] Xinggong Wang, Yongluan Yan, Peng Tang, Xiang Bai, and Wenyu Liu. Revisiting multiple instance neural networks. *Pattern Recognition*, 74:15–24, 2018.
- [37] Xin Xu and Eibe Frank. Logistic regression and boosting for labeled bags of instances. In *Advances in Knowledge Discovery and Data Mining*, pages 272–281, 2004.
- [38] Chhavi Yadav and Léon Bottou. Cold case: The lost mnist digits. In *Advances in Neural Information Processing Systems 32*, 2019.
- [39] Yongluan Yan, Xinggong Wang, Xiaojie Guo, Jiemin Fang, Wenyu Liu, and Junzhou Huang. Deep multi-instance learning with dynamic pooling. In *Proceedings of The 10th Asian Conference on Machine Learning*, volume 95, pages 662–677, 2018.
- [40] Hongkun Yu, Chen Chen, Xianzhi Du, Yeqing Li, Abdullah Rashwan, Le Hou, Pengchong Jin, Fan Yang, Frederick Liu, Jaeyoun Kim, and Jing Li. TensorFlow Model Garden. <https://github.com/tensorflow/models>, 2020.
- [41] Sergey Zagoruyko and Nikos Komodakis. Learning to compare image patches via convolutional neural networks. In *Proceedings of the IEEE Conference on Computer Vision and Pattern Recognition (CVPR)*, June 2015.

-
- [42] Jure Zbontar, Li Jing, Ishan Misra, Yann LeCun, and Stéphane Deny. Barlow twins: Self-supervised learning via redundancy reduction. In *Proceedings of the 38th International Conference on Machine Learning, ICML 2021*, volume 139, pages 12310–12320, 2021.
 - [43] Qi Zhang and Sally Goldman. Em-dd: An improved multiple-instance learning technique. In *Advances in Neural Information Processing Systems*, volume 14, 2001.
 - [44] Zhi-Hua Zhou. A brief introduction to weakly supervised learning. *National Science Review*, 5(1):44–53, 2017.
 - [45] Zhi-Hua Zhou, Yu-Yin Sun, and Yu-Feng Li. Multi-instance learning by treating instances as non-i.i.d. samples. In *International Conference on Machine Learning*, pages 1249–1256, 2009.